Oceanic crust components in continental basalts from Shuangliao, Northeast China: Derived from the mantle transition zone?

Yi-Gang Xu [a,*], Hui-Huang Zhang [a,b], Hua-Ning Qiu [a], Wen-Chun Ge [c], Fu-Yuan Wu [b]

[a] State Key Laboratory of Isotope Geochemistry, Guangzhou Institute of Geochemistry, Chinese Academy of Sciences, Guangzhou, 510640, China
[b] State Key Laboratory of Lithospheric Evolution, Institute of Geology and Geophysics, Chinese Academy of Sciences, Beijing, 100029, China
[c] College of Earth Sciences, Jilin University, Changchun, 130061, China

ARTICLE INFO

ABSTRACT

Basaltic rocks from Shuangliao, northeast China include basanite, alkali olivine basalt, transitional basalt and sub-alkaline diabase. Ar–Ar dating shows that the basanites and alkali olivine basalts formed earlier (48.5–51 Ma) than the transitional basalts and diabases (43–41.6 Ma). These rocks have the highest Fe_2O_3 contents (13.4–14.6 wt.%) and lowest ($^{87}Sr/^{86}Sr$)$_i$ ratios (<0.703) among the Cenozoic basalts from eastern China. On a primitive-mantle normalized variation diagram, they show positive Eu, Sr, Nb and Ta anomalies, and depletion in very incompatible elements (Rb, Ba, Th, U), reminiscent of HIMU-type oceanic island basalts. In particular, the basanites possess noticeable negative K anomalies. Nevertheless, their Pb isotopic compositions ($^{206}Pb/^{204}Pb = 18.13$–18.34) do not show the high time-integrated $^{238}U/^{204}Pb$ mantle component expected for a HIMU basalt. On a $^{206}Pb/^{204}Pb$ versus $^{207}Pb/^{204}Pb$ diagram, most samples straddle the Northern Hemisphere Reference Line (NHRL), in salient contrast to the majority of Chinese Cenozoic basalts, which plot above the NHRL. These data, as well as a comparison with high-pressure experimental melts, are consistent with the presence of young subducted oceanic crust (SOC) in the source of Shuangliao basalts. Varying ($^{87}Sr/^{86}Sr$)$_i$, La/Nb and Eu/Eu* with rock-type suggests that the upper oceanic crust (with variable amount of lower oceanic crust) was preferentially sampled by earlier (51–48 Ma), highly alkaline rocks, whereas the lower oceanic crust was predominantly sampled in later (41–43 Ma) transitional basalts and diabases. This temporal trend is attributed to the differential melting of a heterogeneous source in association with lithospheric thinning, during which fusible upper oceanic crust melted earlier than lower oceanic crust and peridotites. We postulate that the SOC components may have been derived from the seismically detected stagnant Pacific slab within the mantle transition zone. This hypothesis is supported by the same Indian MORB-like isotopic composition being found in the Shuangliao basalts and in the extinct Izanaghi–Pacific plate of NW Pacific. The latter has been subducting underneath the eastern Asian continent since the early Cretaceous.

1. Introduction

Identification of components contributing to the genesis of mafic magmas is one of the major geochemical challenges in understanding the dynamics of the Earth's mantle (Zindler and Hart, 1986). Despite much work in this area, the origin of alkaline basalts remains a matter of heated debate. Earlier experiments have demonstrated that alkali basalts form at higher pressure via a smaller degree of partial melting of peridotites compared to tholeiites (Green and Ringwood, 1967; Kushiro, 2001). However, it has been repeatedly stated in recent years that melts derived from a peridotitic source generally do not mimic oceanic island basalts (OIB) and alkaline basalts. Pyroxenite or eclogite, carbonated peridotites and eclogites are considered as possible candidates instead of peridotites for the source of alkaline basalts (e.g., Hirschmann and Stopler, 1996; Kogiso et al., 2003; Dasgupta et al., 2006). However, the role of pyroxenites in genesis of oceanic basalts has recently been questioned by Putirka et al. (2011).

Two competing opinions exist regarding the petrogenetic models of alkaline basalts. One attributes the peculiar geochemical feature of alkali basalts to recycled oceanic crust in the magma source (Hofmann and White, 1982; Hirschmann and Stopler, 1996; Stracke et al., 2005; Dasgupta et al., 2010). It is widely accepted that oceanic crust can be recycled through the mantle as a result of subduction to the upper–lower mantle or to the core–mantle boundary and then subsequent return to the surface at mid ocean ridges (Hirschmann and Stopler, 1996) or mantle plumes (Hofmann and White, 1982), although the physical/petrologic carrier of this crustal component remain poorly characterized.

The other involves mantle metasomatism (Halliday et al., 1990; Niu and O'Hara, 2003; Pilet et al., 2008), in which trace element enrichment in OIB is due to melting of veins consisting of amphiboles

* Corresponding author at: Guangzhou Institute of Geochemistry, Chinese Academy of Sciences, 510640 Wushan, Guangzhou, China. Tel.: +86 20 85290109; fax: +86 20 85290261.
E-mail address: yigangxu@gig.ac.cn (Y.-G. Xu).

and other metasomatic phases. These phases, which are stable in the lithospheric mantle, are produced by infiltration of small degree partial melts. This model implies a lithospheric origin of alkaline magmas, as suggested by Halliday et al. (1990) in case of Cameroon line basalts. Niu and O'Hara (2003) envisioned a different scenario in that metasomatized lithosphere was subducted into the mantle, and then recycled to become a source of OIBs.

The Cenozoic intraplate igneous rocks of eastern China are low in volume (<10,000 km^3), are predominantly alkaline and have OIB-like trace element compositions (Song et al., 1990; Zhi et al., 1990; Basu et al., 1991; Zou et al., 2000; Xu et al., 2005; Zhang et al., 2009; Zeng et al., 2011). These studies lead to the conclusion that Cenozoic basalts from North China are dominated by mixing of EMI and DM components, whereas those from South China are dominated by EMII and DM components (e.g., Zou et al., 2000). So far, HIMU, which is frequently cited as evidence for oceanic crustal recycling, has not been reported from Chinese Cenozoic basalts. This remains puzzling because the influence of the Pacific subduction on the geologic evolution of the eastern Asian continent has long been recognized from various observations (Wu et al., 2005; Huang and Zhao, 2006; Xu, 2007). The solution to this dilemma is highly relevant to assess the role of subduction of Pacific plate (i.e., direct versus indirect) in generating intraplate magmatism in eastern China.

This paper presents geochemical evidence for involvement of subducted oceanic crust in Eocene basalts from Shuangliao, NE China. We speculate that the horizontally distributed, subducted Pacific slab in the mantle transition zone underneath the eastern Asian continent (Huang and Zhao, 2006), rather than a mantle plume, may serve as source of this crustal component. A model involving differential melting of a heterogeneous source is proposed to account for the temporal change in lava composition.

2. Geologic setting and sampling

2.1. Geologic setting

In China, Cenozoic intraplate basalts are largely concentrated in the eastern continental margin, extending from Heilongjiang province in the north to Hainan island in the south (Fig. 1a). They constitute an important part of the volcanic belt of the western circum-Pacific rim and are one of the world's presently active tectono-magmatic regions (Zhou and Armstrong, 1982; Fan and Hooper, 1991; Liu et al., 2001). Northeast China, in the eastern part of the Paleozoic Central Asian Organic Belt (Fig. 1a), is a composite fold belt formed by amalgamation of several minor blocks during subduction and collision between the Siberian craton and the North China craton (Sengör et al., 1993). The final suturing of these two continents was not complete until the Jurassic (Zhao et al., 1990). Cenozoic volcanic rocks in northeast China are voluminous compared to those outcropping in North China and South China. Hundreds of volcanoes have erupted basalts over an area of 50,000 km^2 and are exposed in the Songliao graben and on its flanks, and along the Yilan–Yitong and Fushun–Mishan faults (Fig. 1a). The volcanic activity in this region occurred in three episodes with related to the opening of the Japan Sea. Prior to Japan Sea rifting, volcanic eruptions started in the Songliao basin and at Datun near Changchun in late Cretaceous (86–90 Ma; Liu et al., 2001; Zhang et al., 2006), then in the early Cenozoic (40–50 Ma) migrated flankward. The Eocene volcanism in Shuangliao, which forms the objective of this study, may represent the type activity in this episode. No volcanism is reported during the opening of Japan Sea (32–16 Ma, Jolivet et al., 1994), probably due to the compressional stress created by spreading of Japan Sea on the eastern Asian continental margin. After cessation of the Japan Sea opening, volcanism resumed in NE China with greatest intensity occurring on both flanks particularly along the Yilan–Yitong fault at 14–13 Ma and
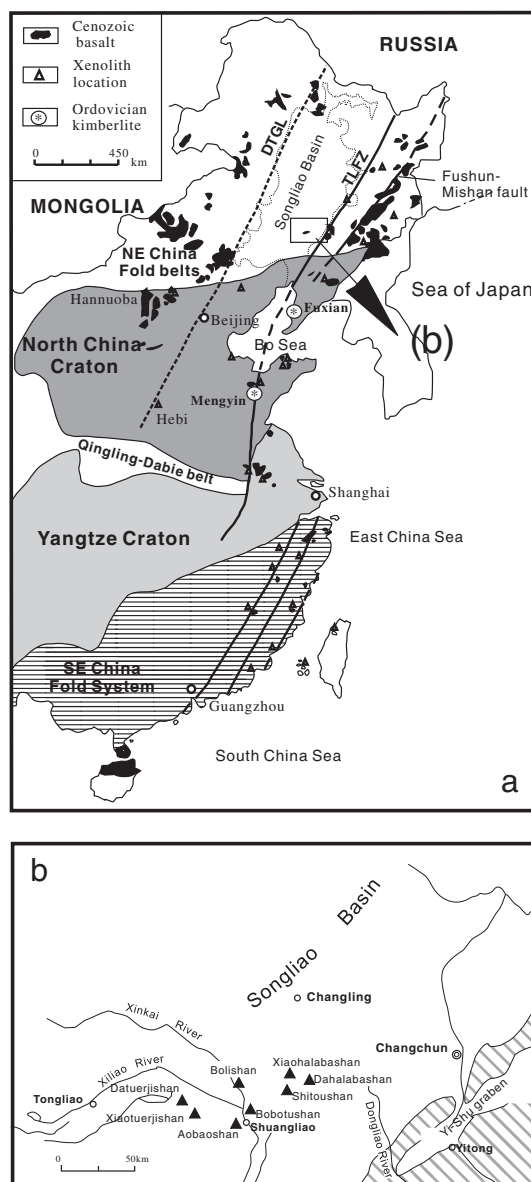

Fig. 1. Simplified tectonic scheme and distribution of Cenozoic basalts in eastern China and the location of the Shuangliao volcanic field southern edge of the Songliao basin, northeastern China. Note that eastern China is cut by two major geological and geophysical linear zones — Tan-Lu fault zone (TLFZ) to the east and Daxinganlin–Taihang gravity lineament (DTGL) to the west.

subsequently the Fushun–Mishan fault between 11 and 7 Ma (Liu et al., 1992, 2001).

Cenozoic volcanism in NE China is dominated by alkali basalts with subordinate tholeiites. Most contain abundant mantle xenoliths that have attracted numerous studies (Xu et al., 1993, 1998, 2003; Zhang et al., 2000; Wu et al., 2003; Yu et al., 2009, 2010). Comparatively few systematic geochemical studies have been carried out on the volcanic rocks (Chen et al., 2007) with the notable exception of the potassic rocks from Wudalianchi (Zhang et al., 1991; Chen et al., 2003). The samples investigated in this study were collected from the Shuangliao volcanic field along southeastern edge of the Songliao basin (Fig. 1b). The Shuangliao volcanic field consists of eight volcanoes: Bobotushan, Naobaoshan, Bolishan, Dahalabashan, Xiaohalabashan, Datuerjishan, Xiaotuerjishan, and Shitoushan. The eruptive rocks vary from dolerites, alkaline olivine basalt and basanite, with K–Ar ages ranging

Table 1
Major and trace element composition of the Shuangliao basalts.

	Bobotushan			Aobaoshan				Bolishan			
Ar–Ar age (Ma)	50.1 ± 0.8			48.5 ± 0.8				49.7 ± 0.2			
Sample	BBT-1	BBT-3	BBT-4	NBS-1	NBS-2	NBS-3	NBS-4	BLS-1	BLS-2	BLS-4	BLS-5
Rock type	BAS	BAS	BAS	BAS	BAS	BAS	BAS	BAS	BAS	BAS	BAS
SiO_2 (wt.%)	42.10	42.83	42.66	43.30	42.84	42.77	43.02	46.25	45.30	45.43	44.68
TiO_2	2.92	2.90	2.98	2.90	2.84	2.87	2.85	2.28	2.33	2.31	2.31
Al_2O_3	12.51	12.58	12.81	12.84	12.44	12.59	12.50	12.80	12.91	12.67	12.50
Fe_2O_3T	13.99	13.82	13.77	14.21	13.81	14.31	14.00	13.90	13.84	14.11	13.92
MnO	0.18	0.18	0.18	0.18	0.18	0.18	0.18	0.18	0.18	0.19	0.18
MgO	11.39	11.76	11.35	11.96	11.79	12.23	12.33	11.08	11.67	11.87	12.48
CaO	9.13	8.78	9.52	9.56	9.52	10.13	9.81	7.93	7.79	7.75	7.73
Na_2O	3.65	3.68	3.03	2.52	2.74	2.66	2.93	2.66	2.86	2.69	2.64
K_2O	1.34	1.28	1.48	1.67	1.20	1.23	1.09	2.05	2.10	2.02	1.99
P_2O_5	0.72	0.74	0.63	0.63	0.61	0.62	0.61	0.71	0.73	0.74	0.73
LOI	2.80	1.76	2.20	1.26	1.40	0.94	1.13	0.59	0.64	0.78	1.09
Total	100.72	100.29	100.60	101.02	99.37	100.53	100.46	100.43	100.34	100.56	100.24
Mg#	65.6	66.5	65.8	66.3	66.6	66.6	67.3	65.1	68.0	66.3	67.7
Q	–	–	–	–	–	–	–	–	–	–	–
Or	8.2	7.8	9.0	10.0	7.3	7.4	6.6	12.3	12.6	12.1	12.0
Ab	8.4	11.2	8.8	8.7	11.6	8.1	10.0	19.2	16.7	16.9	15.0
An	14.3	14.4	17.5	19.1	18.7	19.1	18.1	17.2	16.4	16.8	16.7
Ne	12.7	11.3	9.5	7.0	6.7	8.0	8.2	2.0	4.2	3.3	4.2
Di	22.4	20.5	21.7	20.1	21.0	22.5	22.2	14.6	14.5	14.0	14.2
Hy	–	–	–	–	–	–	–	–	–	–	–
Ol	23.4	24.4	23.1	24.9	24.5	24.7	24.8	25.6	25.1	27.5	28.5
Mt	3.2	3.1	3.1	3.2	3.2	3.2	3.2	3.1	4.3	3.2	3.1
Il	5.7	5.7	5.8	5.6	5.6	5.5	5.5	4.4	4.5	4.5	4.5
Ap	1.7	1.8	1.5	1.5	1.5	1.5	1.4	1.7	1.7	1.7	1.7
Ti (ppm)	17,318	16,104	17,367	16,334	16,694	17,017	16,516	13,172	13,015	12,515	12,436
V	236	221	248	239	248	252	242	153	154	150	154
Mn	1396	1297	1380	1388	1374	1430	1422	1380	1364	1295	1335
Co	57.9	53.4	59.2	59.3	63.3	59.9	63.5	53.4	53.9	49.4	52.8
Ni	263	250	254	279	297	291	303	322	320	382	363
Rb	24.2	24.2	27.7	21.9	19.1	17.4	23.4	31.8	28.5	27.4	29.1
Sr	810	791	775	688	685	753	719	915	884	801	863
Y	19.4	19.1	19.8	19.7	19.4	19.7	19.8	18.9	18.2	17.4	18.2
Zr	241	257	234	216	215	213	215	255	254	301	267
Nb	67.4	72.2	71.7	59.3	59.1	61.8	61.0	64.4	66.0	66.7	68.2
Ba	340	339	323	360	336	324	336	358	335	338	349
La	40.6	42.3	36.6	34.8	33.4	33.6	33.7	43.5	43.1	44.0	42.8
Ce	81.0	83.0	72.3	69.4	67.1	68.6	68.1	85.1	85.1	86.6	85.0
Pr	10.12	10.12	8.98	8.80	8.30	8.41	8.49	10.43	10.13	10.52	10.30
Nd	39.3	39.4	36.0	35.4	34.6	34.0	33.7	41.4	40.2	40.3	40.7
Sm	7.79	7.42	7.06	6.89	6.45	6.45	6.83	7.86	7.47	7.69	7.69
Eu	2.55	2.51	2.37	2.35	2.25	2.27	2.30	2.64	2.62	2.61	2.67
Gd	6.74	6.50	6.32	6.64	6.00	6.03	6.26	6.63	6.85	6.78	6.81
Tb	0.96	0.94	0.92	0.95	0.90	0.92	0.91	0.97	0.95	0.88	0.99
Dy	4.91	4.45	4.48	4.75	4.48	4.70	4.51	4.53	4.49	4.20	4.40
Ho	0.85	0.79	0.78	0.83	0.80	0.82	0.80	0.79	0.75	0.69	0.74
Er	1.96	1.78	1.86	1.96	1.83	1.90	1.86	1.73	1.62	1.62	1.59
Tm	0.25	0.24	0.25	0.24	0.24	0.24	0.25	0.22	0.21	0.19	0.20
Yb	1.39	1.29	1.39	1.30	1.31	1.28	1.35	1.17	1.12	1.06	1.05
Lu	0.19	0.17	0.20	0.19	0.18	0.19	0.19	0.17	0.15	0.15	0.16
Hf	6.03	5.84	5.77	5.30	5.26	5.29	5.26	6.29	6.43	5.68	6.12
Ta	4.09	4.06	6.73	3.37	3.34	3.38	3.42	3.77	3.77	4.18	4.24
Th	5.24	4.95	4.60	4.32	4.11	4.26	4.33	5.54	5.47	4.85	4.99
U	1.67	1.61	1.42	1.37	1.26	1.27	1.25	1.72	1.61	1.43	1.52
$\sum$ REE	198.6	200.9	179.5	174.5	167.8	169.4	169.2	207.1	204.8	207.3	205.0
(La/Yb)N	19.8	22.4	17.9	18.2	17.4	17.8	16.9	25.3	26.2	28.1	27.8
Zr/Nb	3.6	3.6	3.3	3.6	3.6	3.5	3.5	4.0	3.8	4.5	3.9
La/Nb	0.60	0.59	0.51	0.59	0.57	0.54	0.55	0.68	0.65	0.66	0.63
Ba/Nb	5.0	4.7	4.5	6.1	5.7	5.2	5.5	5.6	5.1	5.1	5.1
Ba/Th	64.9	68.5	70.3	83.5	81.6	76.1	77.6	64.7	61.2	69.6	69.9
Rb/Nb	0.36	0.34	0.39	0.37	0.32	0.28	0.38	0.49	0.43	0.41	0.43
Th/Nb	0.08	0.07	0.06	0.07	0.07	0.07	0.07	0.09	0.08	0.07	0.07
Th/La	0.13	0.12	0.13	0.12	0.12	0.13	0.13	0.13	0.13	0.11	0.12
Nb/U	40.3	44.8	50.6	43.3	46.8	48.7	48.7	37.4	41.1	46.7	44.8

Note: BAS = Basanite; AOB = alkali olivine basalt; TB = Transitional basalt; DIA = diabase.

Dahalabashan				Xiaohalabashan				Xiaotuerjishan				Datuerjishan		
51.0 ± 0.5				50.9 ± 0.4				43.0 ± 0.4				41.6 ± 0.3		
DHLB-1	DHLB-5	DHLB-8	DHLB-9	XHLB-1	XHLB-2	XHLB-5	XHLB-7	XTJ-1	XTJ-2	XTJ-6	XTJ-4	DTJ-2	DTJ-5	DTJ-1
AOB	AOB	AOB	AOB	AOB	AOB	AOB	AOB	THB	THB	THB	THB	DIA	DIA	DIA
47.40	47.90	47.01	47.72	46.51	45.75	46.76	46.60	47.06	47.01	47.01	47.01	48.02	48.51	48.88
1.81	1.93	2.03	1.87	2.06	1.86	1.99	1.84	2.03	2.10	2.28	2.15	1.97	2.09	1.60
14.07	14.58	14.54	14.41	14.47	14.22	14.21	14.16	13.94	14.07	14.36	14.08	18.16	18.21	18.69
14.17	13.91	14.56	14.03	14.33	14.21	14.11	14.20	13.76	13.77	13.44	13.83	9.68	9.84	8.03
0.19	0.18	0.19	0.19	0.19	0.18	0.19	0.19	0.18	0.18	0.17	0.18	0.12	0.12	0.10
9.32	9.01	9.39	8.71	8.51	8.86	8.88	9.55	10.72	10.21	9.49	10.26	4.34	4.20	4.25
9.11	8.83	9.12	9.00	8.35	8.36	8.04	8.40	9.15	9.25	9.18	9.19	10.66	10.68	10.38
2.88	2.72	2.75	3.10	3.34	3.02	3.29	3.04	2.42	2.35	2.52	2.48	3.45	3.32	3.51
1.14	1.35	1.27	1.27	1.83	1.43	1.66	1.46	1.11	1.18	1.30	1.18	1.34	1.42	1.35
0.45	0.33	0.33	0.52	0.53	0.44	0.52	0.44	0.27	0.28	0.33	0.30	0.31	0.38	0.24
−0.10	−0.20	−0.23	−0.03	0.30	2.20	0.53	0.23	−0.10	0.07	0.27	−0.03	2.25	1.54	3.14
100.43	100.54	100.94	100.79	100.40	100.53	100.18	100.11	100.54	100.45	100.37	100.62	100.30	100.31	100.18
60.6	60.2	60.1	59.2	59.9	59.3	61.3	61.1	64.6	63.4	62.3	63.4	51.2	49.9	57.1
–	–	–	–	–	–	–	–	–	–	–	–	–	–	–
6.8	8.0	7.5	7.5	10.9	8.7	10.0	8.7	6.6	7.0	7.8	7.0	8.1	8.6	8.3
24.0	23.1	21.3	24.5	20.6	21.4	23.4	21.4	20.6	20.0	21.6	21.1	25.0	26.1	28.7
22.2	23.7	23.6	21.7	19.3	21.6	19.4	21.0	24.0	24.5	24.3	23.9	31.0	31.2	32.4
0.3	–	1.1	1.0	4.3	2.6	2.6	2.5	–	–	–	–	2.7	1.4	1.1
16.6	14.8	15.9	16.1	15.5	14.8	14.4	15.0	16.1	16.1	15.9	16.2	17.6	16.8	15.8
–	2.9	–	–	–	–	–	–	2.7	3.8	2.0	1.6	–	–	–
22.5	20.0	22.7	21.2	19.7	22.9	20.8	23.6	22.5	20.7	20.3	22.3	8.8	8.8	7.4
3.2	3.1	3.2	3.1	4.5	3.2	4.4	3.2	3.1	3.1	3.0	3.1	2.2	2.2	2.6
3.5	3.7	3.9	3.6	4.0	3.6	3.8	3.5	3.9	4.0	4.4	4.1	3.8	4.1	3.2
1.1	0.8	0.8	1.2	1.2	1.1	1.2	1.0	0.6	0.7	0.8	0.7	0.7	0.9	0.6
10,128	11,329	11,448	10,812	11,760	11,368	11,259	10,815	11,170	11,612	12,897	12,484	11,503	12,739	9995
161	186	195	171	170	175	165	171	177	190	202	213	213	201	170
1405	1296	1452	1468	1360	1442	1460	1430	1230	1257	1233	1343	890	990	818
50.4	48.7	53.5	49.3	48.2	51.3	52.4	55.2	54.5	54.4	51.1	58.8	28.8	30.6	31.0
191	179	189	179	158	178	186	194	209	206	190	232	57	52	55
17.6	22.6	20.5	19.5	30.0	24.7	29.3	24.9	12.7	13.8	16.7	15.1	16.8	17.0	18.6
599	455	335	618	672	619	678	661	314	318	338	326	694	712	713
17.9	18.1	17.6	19.9	19.7	18.5	18.9	17.2	14.1	15.0	17.0	15.8	14.1	15.3	12.8
143	165	155	168	235	203	233	204	130	138	156	143	149	154	151
32.8	35.3	34.0	38.7	53.5	43.9	51.1	44.5	23.7	25.4	28.5	25.7	28.0	29.9	27.2
200	255	213	221	343	235	300	257	159	165	182	165	223	253	209
26.0	22.5	19.8	30.6	34.0	28.2	33.3	28.0	13.3	14.1	16.3	14.4	16.9	17.4	14.5
52.5	46.0	39.6	58.7	67.7	56.5	65.8	56.2	28.9	29.8	34.0	31.3	35.0	37.4	29.8
6.26	5.79	5.07	7.31	8.35	6.92	8.18	6.80	3.70	3.86	4.53	4.03	4.50	4.88	3.80
25.8	23.3	20.9	29.6	33.0	27.6	32.3	27.5	15.7	16.6	18.8	17.7	19.0	20.7	16.0
5.24	4.80	4.29	5.89	6.41	5.59	6.39	5.62	3.64	3.84	4.31	4.20	4.15	4.72	3.50
1.93	1.74	1.65	2.18	2.26	2.02	2.22	2.01	1.44	1.46	1.71	1.56	1.67	1.78	1.46
4.98	4.82	4.64	5.42	5.86	5.33	5.85	5.18	3.93	3.90	4.54	4.30	4.13	4.46	3.66
0.76	0.76	0.71	0.87	0.89	0.81	0.87	0.80	0.62	0.63	0.71	0.68	0.65	0.69	0.55
3.99	4.04	3.85	4.57	4.43	4.26	4.28	3.94	3.29	3.30	3.81	3.74	3.24	3.50	2.81
0.72	0.74	0.75	0.80	0.78	0.75	0.75	0.69	0.58	0.62	0.70	0.67	0.58	0.62	0.54
1.75	1.80	1.74	1.95	1.89	1.83	1.78	1.61	1.40	1.42	1.62	1.63	1.37	1.45	1.25
0.23	0.26	0.28	0.28	0.26	0.26	0.25	0.23	0.20	0.21	0.22	0.22	0.19	0.19	0.17
1.41	1.46	1.52	1.59	1.53	1.45	1.38	1.30	1.09	1.15	1.29	1.33	1.06	1.13	0.98
0.20	0.23	0.24	0.23	0.23	0.22	0.21	0.20	0.17	0.17	0.19	0.19	0.15	0.16	0.14
3.50	4.02	4.00	4.29	5.41	4.86	5.57	4.82	3.28	3.34	3.78	3.80	3.68	3.97	3.67
1.73	1.99	2.05	2.10	3.03	2.55	2.95	2.57	1.36	1.36	1.60	1.87	1.54	1.65	2.56
2.75	3.22	2.95	3.48	4.32	3.77	4.57	4.00	1.49	1.62	1.88	1.85	2.07	2.07	2.14
0.78	0.90	0.89	1.04	1.28	1.06	1.32	1.13	0.49	0.50	0.61	0.57	0.62	0.64	0.67
131.7	118.3	105.0	149.9	167.5	141.7	163.5	140.0	78.0	81.1	92.7	85.9	92.6	99.1	79.1
12.5	10.4	8.8	13.0	15.1	13.2	16.4	14.6	8.3	8.3	8.6	7.3	10.8	10.5	10.0
4.4	4.7	4.6	4.3	4.4	4.6	4.6	4.6	5.5	5.4	5.5	5.6	5.3	5.1	5.6
0.79	0.64	0.58	0.79	0.64	0.64	0.65	0.63	0.56	0.55	0.57	0.56	0.60	0.58	0.53
6.1	7.2	6.3	5.7	6.4	5.4	5.9	5.8	6.7	6.5	6.4	6.4	8.0	8.5	7.7
72.5	79.1	72.3	63.5	79.4	62.4	65.7	64.3	106.4	101.5	97.3	89.1	107.8	122.7	97.4
0.54	0.64	0.61	0.50	0.56	0.56	0.57	0.56	0.53	0.54	0.59	0.59	0.60	0.57	0.68
0.08	0.09	0.09	0.09	0.08	0.09	0.09	0.09	0.06	0.06	0.07	0.07	0.07	0.07	0.08
0.11	0.14	0.15	0.11	0.13	0.13	0.14	0.14	0.11	0.11	0.12	0.13	0.12	0.12	0.15
41.9	39.2	38.2	37.2	41.8	41.4	38.7	39.4	48.6	50.6	46.4	45.2	45.5	46.8	40.3

from 86 to 40 Ma (Yu, 1987). These volcanoes carry abundant mantle xenoliths of spinel lherzolites and harzburgites (e.g., Yu et al., 2009).

2.2. Samples and their petrography

The Shuangliao volcanic rocks are classified into four types based on their petrography and major element compositions (Table 1): basanites, alkali olivine basalt, transitional basalt and diabase. There is gradation from high Ne-norms in basanites to low Ne norms in alkali basalts. No normative Ne was found in the transitional basalts or diabases.

The basanites are from Bobotushan, Aobaoshan and Bolishan. Although the samples from Bolishan do not plot within the basanite field on a TAS plot (Fig. 2), they show similar mineralogy and high Ne-norms to the basanites from Bobotushan and Aobaoshan. Accordingly these samples are also grouped with the basanites. The basanites contain olivine xenocrysts (Fo = 0.90–0.91, NiO = 0.37–0.39 wt.%). The dominant phenocrysts (25%) are olivine (Fo = 0.71–0.88) and diopside ($WO_{49-52}EN_{34-39}FS_{12-15}$). The groundmass is composed of olivine, pyroxene, glass and minor Ti-magnetite.

The rocks from Dahalabashan and Xiaohalabashan are alkali olivine basalts. Petrographically they resemble basanites but no olivine xenocrysts are found in this rock type. Phenocryst assemblages are comprised of olivine (Fo = 0.66–0.69), diopside–augite ($WO_{44-49}EN_{37-44}FS_{13-16}$) and minor plagioclase.

In transitional basalts from Xiaotuerjishan, plagioclase becomes the dominant phenocryst (~50%). Other subordinate phenocrysts include olivine (~20%) and augite. Diabase sills occur at Datuerjishan. The mineral assemblage consists of 60% plagioclase (An = 52–63), and ~30% diopside ($WO_{46-47}EN_{36-40}FS_{13-19}$), with minor amounts of olivine (Fo = 0.57–0.71).

3. Analytical methods

The samples were sawed into slabs and the central parts were used for bulk-rock analyses. The rocks were crushed in a steel mortar and ground in a steel mill. Bulk rock abundances of major elements were determined using an X-ray fluorescence spectrometer (XRF) on glass disks at the Guangzhou Institute of Geochemistry, Chinese Academy of Sciences (GIGCAS), following analytical procedures described by Goto and Tatsumi (1996). Pre-ignition was used to determine the loss on ignition (LOI) prior to major element analyses. Analytical uncertainties for majority of major elements analyzed were estimated at less than 1% from repeatedly analyzed U.S.G.S. standards BHVO-2, MRG-1 (basalt) and W-2 (diabase). The measured values of international standards are in satisfactory agreement with the recommended values (Table 2). Bulk-rock trace element data [rare earth elements (REE), Sc, Ti, V, Cr, Cs, Sr, Y, Ba, U, Rb, Th, Pb, Zr, Hf, Nb, Ta] were obtained by inductively coupled plasma-mass spectrometry (ICP-MS) at GIGCAS, following the analytical procedures described by Xu (2002). The powders (~50 mg) were dissolved in distilled HF-HNO$_3$ in Savillex screwtop Telfon breakers at 150 °C for >4 days. Precision for REE and HFSE is estimated to be 5% from repeatedly analyzed U.S.G.S. standards BHVO-1 and W-2 (Xu, 2002).

For Sr–Nd isotopic analyses, sample powders (~100 mg) were dissolved in distilled HF-HNO$_3$ Savillex screwtop Teflon beakers at 150 °C overnight. Sr and REE were separated on columns made of Sr and REE resins from the Eichrom Company using 0.1% HNO$_3$ as elutant. Separation of Nd from the REE fractions was carried out on HDEHP columns with a 0.18 N HCl elutant. The isotopic analyses were performed using a Micromass Isoprobe Multi-Collector ICPMS at GIGCAS. Measured Sr and Nd isotopic ratios were normalized using a $^{86}Sr/^{88}Sr$ value of 0.1194 and a $^{146}Nd/^{144}Nd$ value of 0.7219, respectively. The Sr and Nd blanks during the period of analyses are 0.5 ng and 0.3 ng, respectively. Twenty analyses of standards during the period of analysis are as follows: NBS987 gave $^{87}Sr/^{86}Sr = 0.710243 \pm 14$ (2σ); Shin

Etou gave $^{143}Nd/^{144}Nd = 0.512124 \pm 11$ (2σ), equivalent to a value of 0.511860 for the La Jolla international standard (Tanaka et al., 2004). Detailed analytical procedure can be found in Wei et al. (2002) and Liang et al. (2003).

For Pb isotopic analyses, ~200 mg powder was dissolved in concentrated HF for three days. Pb was separated and purified by conventional cation-exchange techniques (200–400 mesh AG1X8 resin) with diluted HBr as eluant. Pb isotopes were determined using a VG-354 mass spectrometer at the Institute of Geology, Chinese Academy of Sciences (Beijing). Analyses of standard NBS981 during the period of analysis yielded $^{204}Pb/^{206}Pb = 0.0897 \pm 15$, $^{207}Pb/^{206}Pb = 0.91445 \pm 80$, $^{208}Pb/^{206}Pb = 2.16170 \pm 200$.

The $^{40}Ar/^{39}Ar$ dating was carried out at GIGCAS using a GV5400 mass spectrometer following analytical procedures described by Qiu and Jiang (2007). Argon gas was extracted from the sample by step-heating using MIR10 CO$_2$ continuing laser. The released gasses were purified by two Zr/Al getter pumps operated for 5 to 8 min at room temperature and ~450 °C respectively. The background of the sample hold is lower than 2 mV pre-experiment, while the signal for the sample is mostly between 40 and 200 mV. The $^{40}Ar/^{39}Ar$ dating results are calculated and plotted using the ArArCALC software by Koppers (2002). The J-value was 0.00955 as determined by ZBH-2506 biotite (132 Ma) flux monitors.

4. Results

4.1. Ar–Ar geochronology

The $^{40}Ar/^{39}Ar$ dating results for 7 samples from Shuangliao are plotted as age spectrum and $^{40}Ar/^{36}Ar–^{39}Ar/^{36}Ar$ isotope correlation diagrams in Fig. 3. A summary of the results is given in Table 2. In all cases, the plateau age and isochron age are identical within the error. As a consequence, the plateau age spectrum is interpreted to represent the eruption age of the basalts. The basalts from Shuangliao are all Eocene (41.6–51.0 Ma) in age. Most of these dates are in good agreement with previously determined K–Ar ages (Yu, 1987). The exception is the Eocene age obtained for the Datuerjishan sample, which is significantly different from the late Cretaceous age previously obtained by the K–Ar method. The Eocene eruption age of the Shuangliao basalts is distinct from the predominant post-Miocene ages obtained for the Cenozoic basalts from Eastern China. Specifically, five out of seven volcanic cones with high alkalinity were erupted between 51 and 48.5 Ma. Other two cones from Datuerjishan and Xiaotuerjishan, which have transitional to subalkaline characteristics, were emplaced at 41.6 Ma and 43.0 Ma, respectively. Therefore, the alkalinity of the Shuangliao volcanic rocks appears to decrease with time.

4.2. Major and minor elements

The Shuangliao volcanic rocks display a moderate range in SiO$_2$ (42.1–48.9 wt.%) and a relatively large variation in MgO (4.20–12.48 wt.%). The basanites are characterized by high MgO contents (MgO > 11 wt.%), Mg# (65.1–67.7), high Ni and Co contents (250.3–381.6 ppm and 49.4–63.4 ppm, respectively), pointing to their least fractionated nature. These rocks also have high TiO$_2$ (2.28–2.98 wt.%), Fe$_2$O$_3$ (13.8–14.3 wt.%) and relatively low Al$_2$O$_3$ (<13 wt.%) contents. The most fractionated rocks are from Datuerjishan, as attested by their high SiO$_2$ (48.0–48.9 wt.%), Al$_2$O$_3$ (18.2–18.7 wt.%), CaO (10.4–10.7 wt.%), and low MgO (<4.3 wt.%) and Fe$_2$O$_3$ (8.0–9.8 wt.%) contents. These rocks also display very low concentrations of Ni (51.7–54.6 ppm) and Co (28.8–31 ppm). Alkali olivine basalts (AOB) and transitional basalts (TB) are compositionally intermediate between these two extremes. Overall, Ni and Co show positive correlations with MgO for AOB and TB.
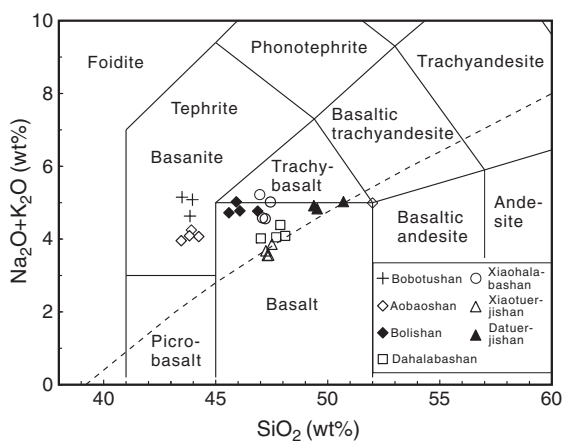
Fig. 2. $Na_2O + K_2O$ versus SiO_2 (Le Bas et al., 1986). Line separating alkali basalts and tholeiites is from McDonald and Katsura (1964).

On the plots of major elements against MgO (Fig. 4), the basanites form compositional trends that are distinct from those defined by the other rock types. For instance, FeO, Al_2O_3, K_2O and P_2O_5 in alkali olivine basalts and transitional basalts correlate negatively with MgO, whereas CaO, Ni and Co correlate positively with MgO. However, although the basanites show a limited range in MgO, they show relatively large variation in SiO_2, CaO, Na_2O and K_2O.

4.3. REE and other incompatible elements

Trace element concentrations in the Shuangliao basalts vary with the rock type, with the highest contents in basanites and the lowest in transitional basalts and diabases (Table 1). The basanites show enrichment of light rare earth elements (LREE) over heavy rare earth elements (HREE) $[(La/Yb)_N = 16.9–28.1]$, and enrichment in Nb and Ta (Fig. 5). These rocks are also characterized by progressive depletion in the most incompatible elements (Rb, Ba, Th, U), forming a positively steep trend with a Nb/Rb of 2–3.6. Other distinctive features include remarkable troughs at K, and noticeable positive Eu and Sr anomalies. These features except Eu and Sr anomalies are very similar to the characteristic of HIMU ocean island basalts (Chauvel et al., 1992; Willbold and Stracke, 2006).

Similar trace element patterns are observed as for the other rock types, but some distinct features are noted as below. (a) although all the rocks from Shuangliao show LREE enrichment over HREE, fractionation between LREE and HREE decreases with decreasing alkali contents (Fig. 5). (b) Weak but remarkable positive Eu anomalies are noted in all the Shuangliao rocks. The extent of this anomaly is minimal in the basanites and is the highest in the transitional basalts and diabases. The fact that the positive Eu anomalies are also present in the basanites, which are free of plagioclase phenocryst, indicates that it is a feature of the source. (c) The extent of K depletion in AOB is smaller than in basanites. K even becomes enriched in transitional basalts and diabase. (d) Compared to the basanites, the depletion of highly incompatible elements relative to Nb is less significant, with

Nb/Rb of 20. TB and diabase are even characterized by enrichment in Rb and Ba.

At a given Th content, the basanites have relatively lower Rb and higher Nb and Ba contents compared to the rest of the samples (Fig. 6a,b,c). Indeed, in these plots the basanites define trends that are different to the other samples, indicative of heterogeneity in the source of the Shuangliao basalts. Source difference between diabases and other rocks is evidenced from the fact that diabases show the least enrichment in incompatible elements despite their low MgO, indicating that diabases cannot have formed by fractional crystallization from other magmas. A broadly negative correlation between Yb and Th is noted for basanites and AOB (Fig. 6d). This is indicative of a compatible character for Yb during the formation of the Shuangliao basalts, consistent with residual garnet in the source of these lavas.

4.4. Sr–Nd–Pb isotopes

The Sr–Nd isotopic compositions of the Shuangliao basalts are relatively homogeneous, with low $(^{87}Sr/^{86}Sr)_i = 0.7030–0.7036$ and high $(^{143}Nd/^{144}Nd)_i = 0.512798–0.512892$ (Table 3). When compared with Cenozoic basalts from other localities in eastern China, the Shuangliao basalts have the lowest $(^{87}Sr/^{86}Sr)_i$ (Fig. 7a). $\varepsilon_{Nd}(t)$ varies with rock type, from 5.2–6.2 for the basanites, to 4.7–5.5 for the alkali olivine basalts, and to 4.2–4.8 for the transitional basalts and diabases. Basanites and other lavas define subparallel trends with positive slopes (Fig. 7b). Consistent with different slopes in bivariant trace element plots (Fig. 6a,b,c) and La/Sm–La plots (Fig. 6f), the Sr–Nd isotope systematics clearly discriminate the basanites from the other lavas, indicating source differences between them.

The Shuangliao basalts show a limited range in Pb isotopic compositions with $^{206}Pb/^{204}Pb$, $^{207}Pb/^{204}Pb$ and $^{208}Pb/^{204}Pb$ ratios ranging from 18.13 to 18.34, 15.46 to 15.50 and 38.18 to 38.58, respectively (Table 3). Pb isotopes seem to vary with rock types, with higher $^{206}Pb/^{204}Pb$ and $^{208}Pb/^{204}Pb$ ratios in the alkali olivine basalts than in the basanites. Unlike the Cenozoic basalts from other parts of eastern China, all but one sample plots along or slightly above the North Hemisphere Reference Line (NHRL, Hart, 1984) (Fig. 7c).

5. Discussion

5.1. Crystal fractionation and crustal contamination

Before basalt compositions can be used to constrain the processes that produce them and the composition of their mantle source region, the effects of low-pressure processes such as crustal contamination and crystal fractionation on lava composition should be evaluated. There is a rough positive correlation between $(^{87}Sr/^{86}Sr)_i$ and SiO_2 (Fig. 8a). In addition, the AOB with low MgO content (~9%) have higher $(^{87}Sr/^{86}Sr)_i$ than the basanites with high MgO (~12 wt.%) (Fig. 8b). All these are in apparent agreement with crustal contamination coupled with fractionation. However, AOB and basanites do not form a coherent trend. Specifically, $(^{87}Sr/^{86}Sr)_i$ of the AOB varies between 0.7033 and 0.7036, irrespective of MgO variation, as do the basanites (Fig. 8b). Similarly a plot of ε_{Nd} against SiO_2 (Fig. 8c) shows a positive correlation for basanites, whereas $\varepsilon_{Nd}(t)$ of the AOB and TB varies between 4 and 5.6,

Table 2
Summary of $^{40}Ar/^{39}Ar$ dating results for the Shuangliao basalts.

Sample no.	Rock type	Locality	Plateau date (Ma)	Intercept date (Ma)	$(^{40}Ar/^{36}Ar)_i$	MSWD
BBT-1	Basanite	Bobotushan	50.1 ± 0.8	48.5 ± 1.2	348.9	13.37
NBS-4	Basanite	Aobaoshan	48.5 ± 0.8	49.5 ± 2.2	211.4	22.22
BLS-4	Basanite	Bolishan	49.7 ± 0.2	49.6 ± 0.5	297.8	3.45
XHLB-1	Alkali olivine basalt	Xiaohalabashan	50.9 ± 0.4	50.4 ± 1.1	322.6	9.63
DHLB-1	Alkali olivine basalt	Dahalabashan	51.0 ± 0.5	50.1 ± 0.5	317.6	2.62
XTJ-2	Transitional basalt	Xiaotu'erjishan	43.0 ± 0.4	42.9 ± 1.0	290.8	7.34
DTJ-2	Diabase	Datu'erjishan	41.6 ± 0.3	41.2 ± 0.5	336.7	5.57

irrespective of SiO$_2$ variation. These observations suggest that the observed isotopic variation reflects source heterogeneity, consistent with the variation in trace element compositions (Fig. 6).

Crustal contamination can also be ruled out by the rough negative correlation between $\varepsilon_{Nd}(t)$ and Sm/Nd (Fig. 8d). If the upper crust was involved in magma genesis, the most contaminated samples with the lowest ε_{Nd} would also display the lowest Sm/Nd (Fig. 8d), because the upper crust is generally characterized by LILE enrichment (low Sm/Nd) and HFSE-depletion. However the Shuangliao samples show a negative correlation, which is reverse of the expected trend for crustal contamination (Fig. 8d). Furthermore, crustal contamination should increase the concentration of highly incompatible elements, accompanied by depletion in Nb–Ta. These expected characteristics are not observed in the Shuangliao basalts, which instead show positive Nb–Ta anomalies and depletion of Rb, Ba, Th and U relative to Nb (Fig. 5). Limited interaction with the lithosphere is also suggested by (a) rapid ascent of magma to the surface, constrained by the presence of peridotite xenoliths in the Shuangliao basanites and alkali basalts (Wu et al., 2003; Yu et al., 2009); and (b) by their high Fe contents (Fig. 4d) and positive Sr–Nd isotopic correlations (Fig. 7b), because interactions with the crust would result in significant lowering in Fe contents and a negative Sr–Nd isotopic correlation.

The basanites have high Ni and Co contents. Their Mg# (>65) approaches that of primary magmas (68–75, Frey et al., 1978). On the plots of major oxides against MgO, no correlation is noted for the basanites, suggesting that fractional crystallization was limited. The alkaline olivine basalts and transitional basalts display relatively low Mg# (59.2–64.6), pointing to a moderately fractionated nature. With decreasing MgO, concentrations of SiO$_2$, K$_2$O, Na$_2$O, TiO$_2$, Al$_2$O$_3$ and trace elements increase gradually, whereas CaO, Ni and Co decrease. These observations suggest various degrees of fractionation of olivine and pyroxenes. It should be noted that compositional difference between the basanites and other samples cannot be accounted for by fractionation, given the absence of a coherent relationship between them (Fig. 6). Such a compositional diversity may have resulted from different degree of partial melting or inherited from the source. For instance, although the decrease in La from basanites though AOB to TB is consistent with control by varying melting degree, the different correlations in La/Sm versus La (Fig. 6f) point to differences in source characteristics.

Although the low MgO, Fe$_2$O$_3$, Ni, Co and high SiO$_2$ contents in the Datu'erjishan diabases may be related to fractional crystallization, their relatively low trace element concentrations (e.g., Th and Yb) are in contradiction with a fractionation model. In fact, the high Al$_2$O$_3$, CaO, Sr concentration and positive Ba and Sr anomalies are consistent with plagioclase accumulation, an interpretation also supported by large amount of plagioclase (>60%) in these samples.

5.2. Source lithology of the Shuangliao basalts

To investigate melting conditions of the mantle and to constrain the source(s) of basalts, a number of high-pressure experiments
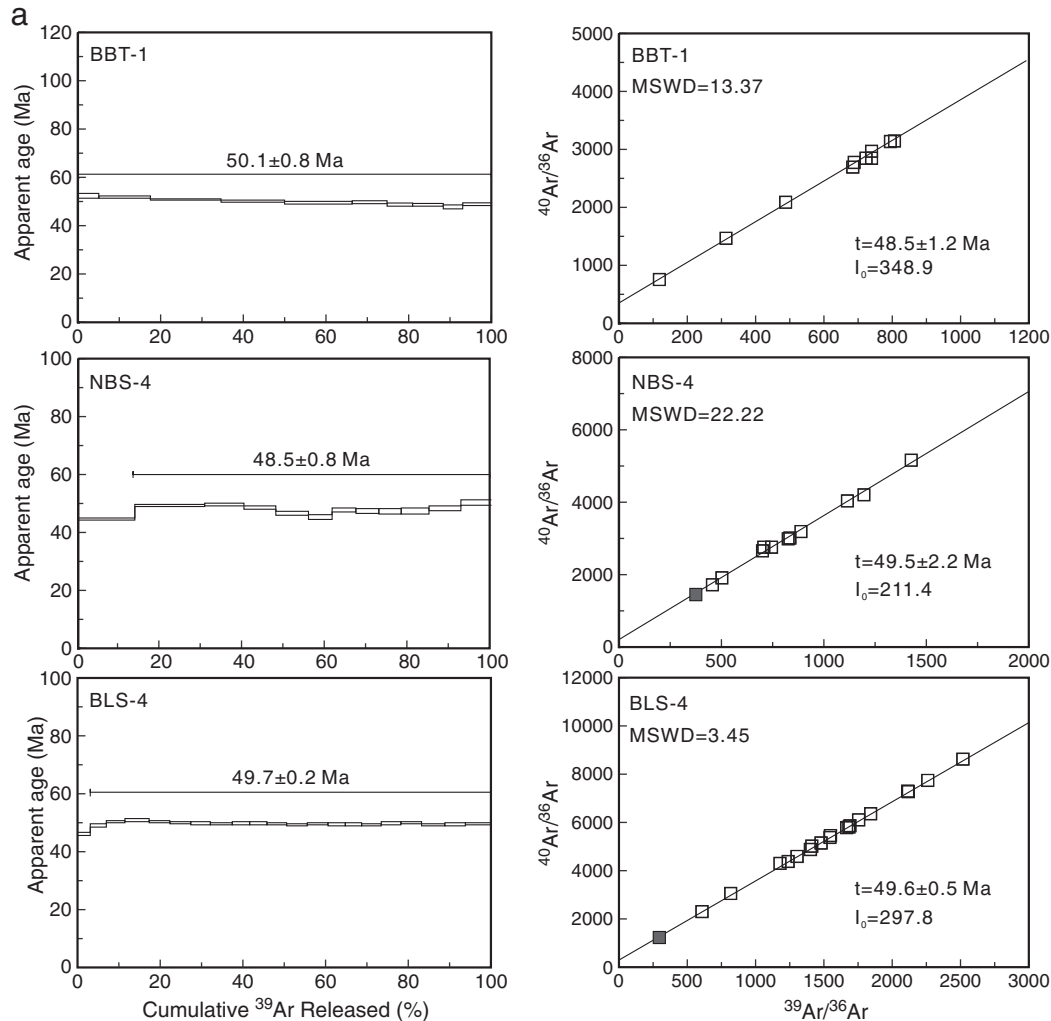

Fig. 3. Ar–Ar age spectra and $^{40}Ar/^{36}Ar$ versus $^{39}Ar/^{36}Ar$ correlation of the whole rocks of the Shuangliao basalts.
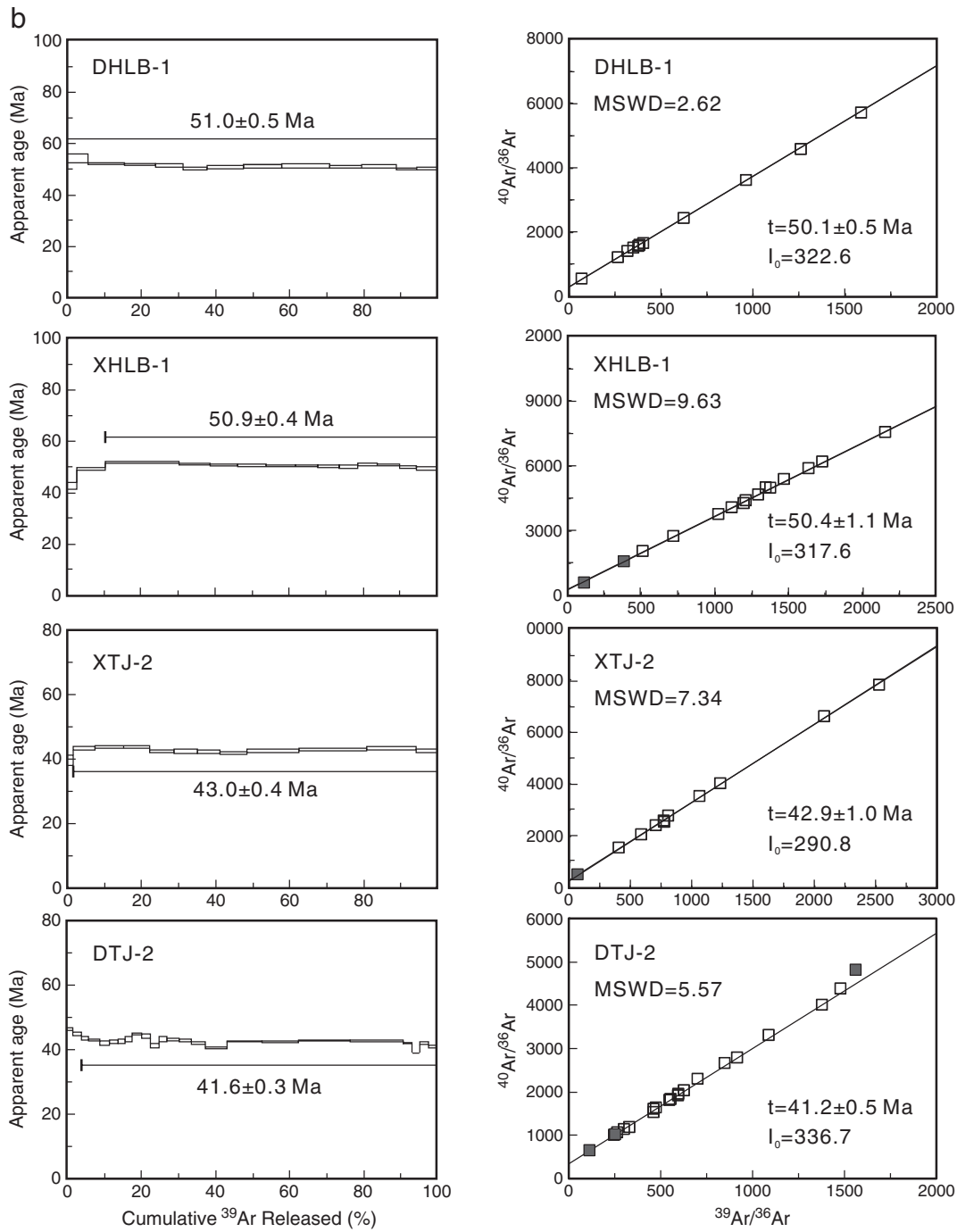
Fig. 3 (*continued*).

have been conceived on a wide array of possible mantle compositions, including volatile-free peridotite (Hirose and Kushiro, 1993; Dasgupta et al., 2007), garnet pyroxenite (Hirschmann et al., 2003), eclogite (Dasgupta et al., 2006; Kogiso and Hirschmann, 2006) and hornblendite (Pilet et al., 2008). Comparison of the major element compositions of the least fractionated Shuangliao basalts with these experimental melts (Fig. 9) can provide important insights into the nature of their source.

In general, low degree melts that are generated at greater depths show lower silica and higher total iron contents than higher degree melts at shallower depth (e.g. Hirose and Kushiro, 1993). Therefore, varying the degree of melting, caused by variable melting depths, generates a negative FeO–SiO$_2$ correlation (Fig. 9a) in both oceanic and continental basalts (e.g., Langmuir et al. 1992). This is not observed in the Shuangliao case, where FeO contents remain constant despite a moderate variation in SiO$_2$ from 42 to 47%. An obliquity with the Fe–Si trend, defined by volatile-free peridotite partial melts, has also been noted for OIB (Dasgupta et al., 2010), suggesting that the compositions of the Shuangliao basalts are not only controlled by melting conditions, but also by source heterogeneity. The observed Fe–Si trend is likely formed as a result of two-component mixing, with low Si-high Fe component from recycled crust (predominant in the basanites) and high Si-high FeO components from a peridotite–eclogite mixture (predominant in the AOB and TB). The different sources for basanites and AOB-TB are also reflected in Fig. 6, in which the basanites have higher Nb/Th and lower Rb/Th ratios than the AOB-TB.
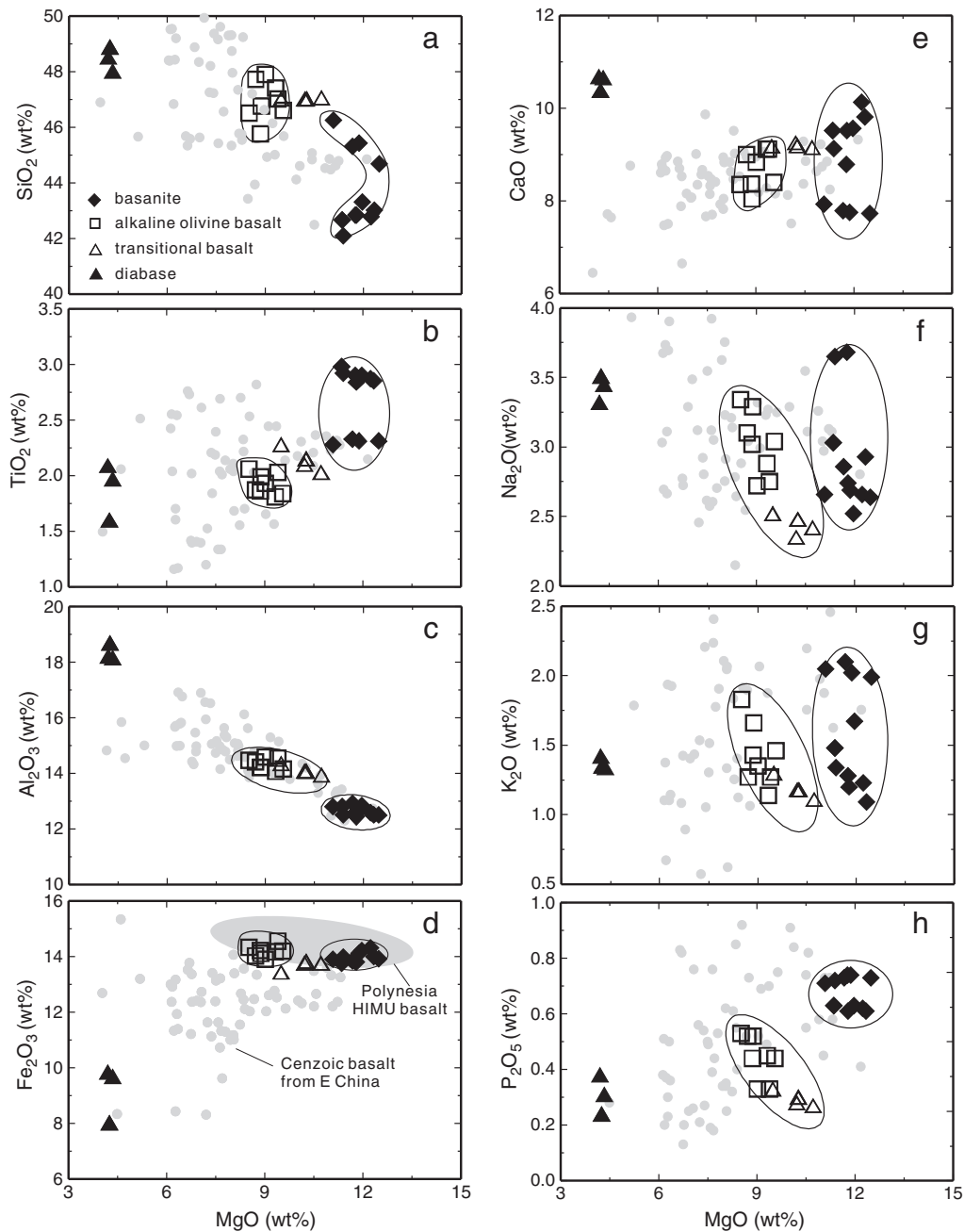
Fig. 4. Variation of SiO_2, TiO_2, TFe_2O_3, Al_2O_3, CaO, Na_2O, K_2O and P_2O_5 versus MgO for Shuangliao basalts. Also shown for comparison are data of Cenozoic basalts from NE China (Basu et al. 1991; Song et al. 1990; Qin et al., unpublished data). The field for Polynesia HIMU basalts is from Chauvel et al. (1992).

The Shuangliao basalts have conspicuously lower SiO_2, higher FeO_T and TiO_2 contents at a given MgO concentration than liquids likely to be derived by crystal fractionation from partial melts of volatile-poor peridotite (Fig. 9b,c,e), thus ruling out a pure peridotitic source for the Shuangliao basalts. In Fig. 9b,c,d, the Shuangliao basanites plot within the field of partial melts of garnet pyroxenites, whereas AOB and transitional basalts lie between the fields for experimental melts of eclogite and peridotite $\pm CO_2$. This suggests a lithologically-mixed source. High ratios of lighter to heavier REE (e.g. Sm/Yb, Tb/Yb) and steep HREE patterns with negative slopes on multi-element diagrams in the Shuangliao basalts are indicative of residual garnet, consistent with a source with eclogite/garnet pyroxenites within a garnet perido-titic matrix.

Given the opposing partitioning behavior of La and Nb in peridotite and pyroxenite-melt systems, the La/Nb ratio can be readily used as a discriminating tracer between pyroxenite and peridotite source signature (Stracke and Bourdon, 2009). All the Shuangliao lavas have low La/Nb<1 (Table 1), indicating melting of a pyroxenite source (Stracke and Bourdon 2009). The basanites trend to have lower La/Nb (0.5–0.68) than the AOB-Transitional basalts (0.58–0.79), suggesting a higher proportion of pyroxenite in the source of basanites than in those of the AOB and TB, consistent with the inference made from comparison with experimental melts. Moreover, there is a broadly positive correlation between La/Nb and Sr isotopic ratios (Fig. 10a).

It should be pointed out that not all comparisons produce coherent results. For instance, the Shuangliao basalts have significantly lower CaO than melts derived from eclogite and garnet pyroxenites (Fig. 9e). Al_2O_3 contents of the Shuangliao basalts overlap with the range of melts derived from garnet pyroxenites and peridotites, and are signifi-cantly higher than eclogite melts (Fig. 9f). This can be related to
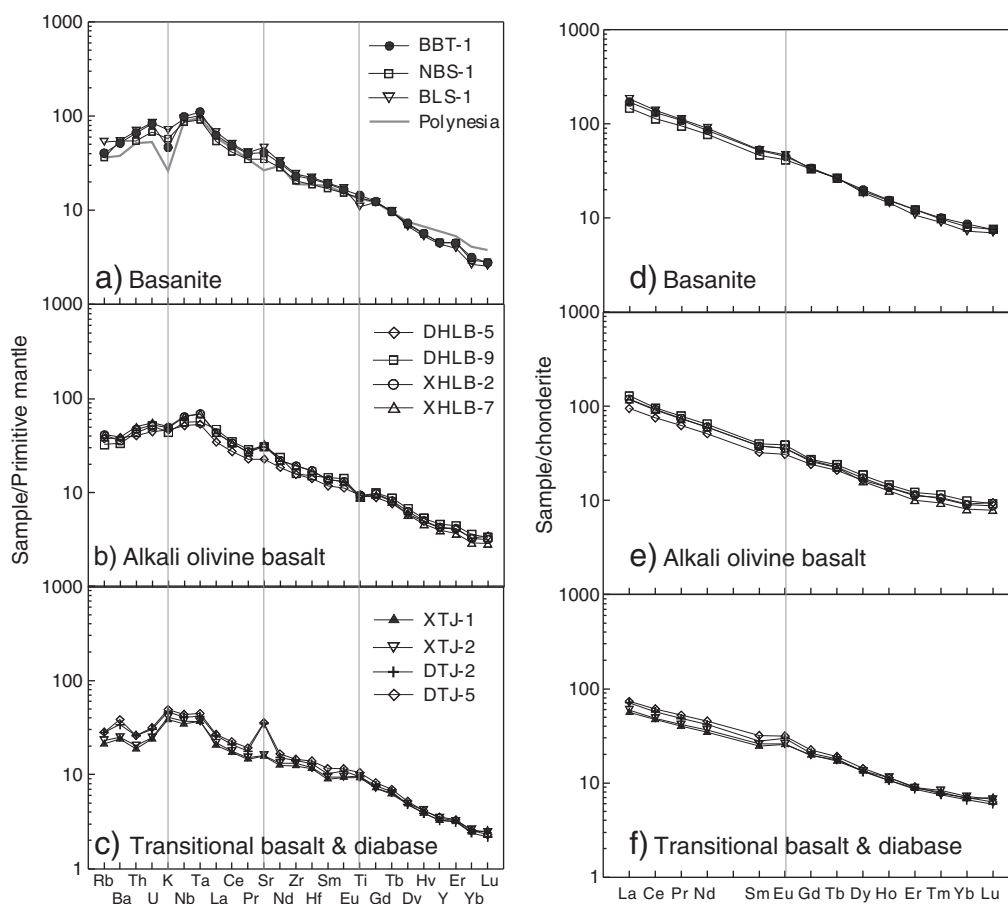
Fig. 5. REE and trace element abundances in whole rocks for the Shuangliao basalts. On the left are spider diagrams normalized by primitive mantle values and on the right are the REE patterns normalized by chondrite values (Sun and McDonough, 1989). Data of Polynesia HIMU basalts is from Chauvel et al. (1992).

insufficient experimental data (due to extremely heterogeneous composition of natural pyroxenites). Alternatively, Putirka et al. (2011) made comparison of Hawaiian lavas with different experimental data and found that experimental partial melts of peridotite cover the observed compositional range. They cast doubt on the pyroxenite model and suggested that a peridotite source cannot be fully ruled out.

With these constraints in mind, the high FeO and TiO$_2$ contents of the Shuangliao basalts clearly distinguish them from peridotite-derived melts. A garnet pyroxenite/eclogite source also gains supporting evidence from recent findings of remnants of oceanic lower crust in the sub-continental lithospheric mantle beneath NE China, now represented by aluminous pyroxenites (Yu et al., 2010).

5.3. Young subducted oceanic crust (SOC) in the source of Shuangliao basalts

5.3.1. Comparison of Shuangliao basalts with HIMU lavas: similarity and difference

Rather than being the product of crustal contamination or crystal fractionation, we suggest that the high FeO contents, low (^{87}Sr/^{86}Sr)$_i$, negative K anomalies, positive Eu and Sr anomalies exhibited by the Shuangliao basalts are characteristics inherited from the source. These characteristics are reminiscent of type HIMU basalts such as the French Polynesian basalts and St. Helena (Chauvel et al., 1992; Willbold and Stracke, 2006). In general, the HIMU basalts are characterized by high Fe contents (Kogiso et al., 1997) and relative deficiency in very incompatible elements such as Rb, Ba, U and Th (Chauvel et al., 1992; Stracke et al., 2005). These key features are shared by the Shuangliao basalts, as highlighted by the essentially same co-variation trends

defined by the Shuangliao basalts and the HIMU basalts form St. Helena (Figs. 5, 6e).

However, the Shuangliao basalts do not show extremely high ^{207}Pb/^{204}Pb as would be expected for typical HIMU components, which are generally attributed to old (~2 Ga) recycled oceanic crust (Zindler and Hart, 1986). The ^{206}Pb/^{204}Pb isotope ratios of the Shuangliao basalts are higher than normal mid-ocean-ridge basalt (N-MORB) but are lower than the HIMU end-member (Fig. 7c). Nevertheless, it should be emphasized that most of them straddle the NHRL. This feature may be related to the recycling of ocean crust for shorter time periods (<1.5 Ga; Thirlwall, 1997). Thirlwall (1997) has shown that the chemical signature responsible for HIMU isotopic compositions has been generated in the mantle either continuously, or on several occasions. It follows that a young subducted oceanic crust (SOC) component is likely present in the source of the Shuangliao basalts.

HIMU-like component in intraplate alkaline basalts may be either in the form of metasomatic assemblage (Niu and O'Hara, 2003; Pilet et al., 2005) or recycled oceanic crusts (Hofmann and White, 1982; Dasgupta et al., 2010). An evaluation of these two alternatives will be given below.

5.3.2. Metasomatized mantle lithosphere?

This model involves infiltration of the upper mantle by small-degree metasomatic melts leading to an enrichment of the incompatible elements (Pilet et al., 2005). The relative enrichment of the metasomatic melts depends on a number of factors such as the initial composition of the mantle they are derived from, the effective partition coefficient values, and the degree of partial melting. Metasomatic melts are generally assumed to be small-degree melts and are
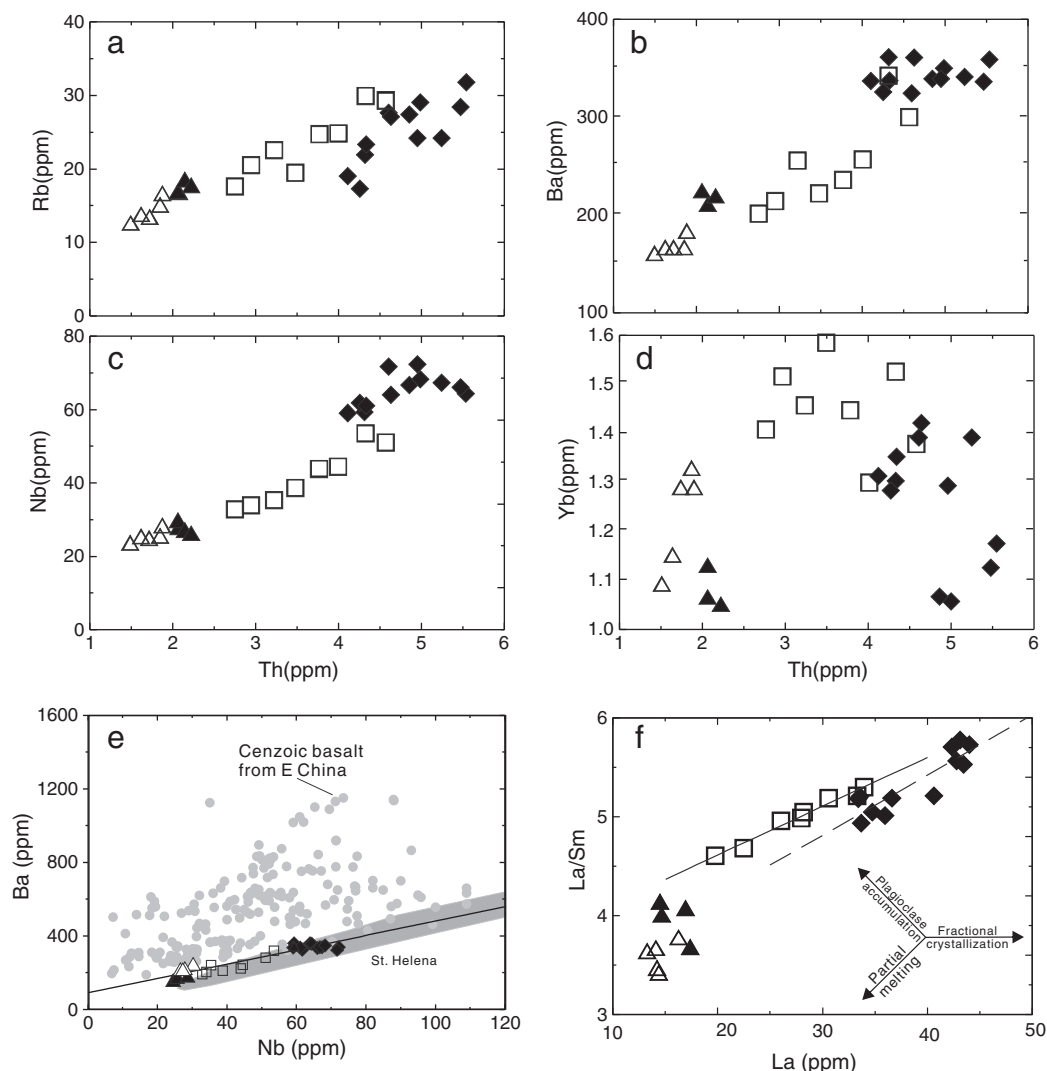
Fig. 6. (a–d) Variation of Rb, Ba, Nb and Yb versus Th; (e) Ba versus Nb; (f) La/Sm versus La. Gray symbols in e stand for Cenozoic basalts from eastern China (Basu et al. 1991; Song et al. 1990; Qin et al., unpublished data). The composition of St. Helena basalts are from Chaffey et al. (1989). Note the compositional similarity between the Shuangliao basalts with type HIMU basalts. Symbols as in Fig. 4.

therefore highly enriched in most incompatible trace elements (Cs, Rb, Ba, Th, U, Nb, Ta) relative to the more compatible elements and the REE (e.g. enrichment of Rb over Sr, and U and Th over Pb). Infiltration and mixing of small amounts (1–2%) of these melts with depleted upper mantle (Salters and Stracke, 2004) generates enriched peridotite sources which can develop isotopic compositions comparable to those of HIMU-type basalts, provided that there is enough time (~2.5 Ga) for the evolution of isotopic signatures after the metasomatic event.

However, this metasomatized model, irrespective of whether metasomatized lithosphere experienced recycling or not, encountered following problems when applied to the Shuangliao basalts.

Table 3
Sr–Nd–Pb isotopic composition of the Shuangliao basalts.

Sample no.	$^{87}Rb/^{86}Sr$	$^{87}Sr/^{86}Sr \pm 2\sigma$	$(^{87}Sr/^{86}Sr)_i$	$^{147}Sm/^{144}Nd$	$^{143}Nd/^{144}Nd \pm 2\sigma$	$(^{143}Nd/^{144}Nd)_i$	$\varepsilon_{Nd}(t)$
BBT-3	0.0885	0.703361 ± 14	0.7033	0.1139	0.512875 ± 7	0.51284	5.2
BLS-5	0.0974	0.703479 ± 13	0.7034	0.1144	0.512929 ± 8	0.51289	6.2
DHLB-1	0.0850	0.703588 ± 13	0.7035	0.1230	0.512872 ± 7	0.51283	5.0
DHLB-8	0.1772	0.703726 ± 13	0.7036	0.1242	0.512896 ± 8	0.51285	5.5
DTJ-5	0.0689	0.703650 ± 11	0.7036	0.1376	0.512858 ± 7	0.51282	4.6
NBS-3	0.0666	0.703089 ± 13	0.7030	0.1148	0.512882 ± 7	0.51285	5.3
NBS-4	0.0940	0.703319 ± 11	0.7032	0.1226	0.512893 ± 7	0.51285	5.4
XHLB-1	0.1289	0.703501 ± 14	0.7034	0.1176	0.512850 ± 8	0.51281	4.7
XHLB-7	0.1089	0.703432 ± 18	0.7034	0.1237	0.512862 ± 8	0.51282	4.8
XTJ-1	0.1166	0.703349 ± 13	0.7033	0.1340	0.512837 ± 6	0.51280	4.2
XTJ-6	0.1427	0.703399 ± 10	0.7033	0.1384	0.512868 ± 6	0.51283	4.8

The isotopic ratios measured are normalized to $^{87}Sr/^{86}Sr = 0.1194$ and $^{146}Nd/^{144}Nd = 0.7219$. Quoted errors for isotopic ratios are 2 SE. Initial $^{87}Sr/^{86}Sr$ ratios are calculated using $\lambda_{Rb} = 1.42 \times 10^{-11}$. Initial $^{143}Nd/^{144}Nd$ ratios and $\varepsilon_{Nd}(t)$ are calculated using $\lambda_{Sm} = 6.54 \times 10^{-12}$ and present-day Bulk Earth values are $^{147}Sm/^{144}Nd = 0.1967$, $^{143}Nd/^{144}Nd = 0.512638$.

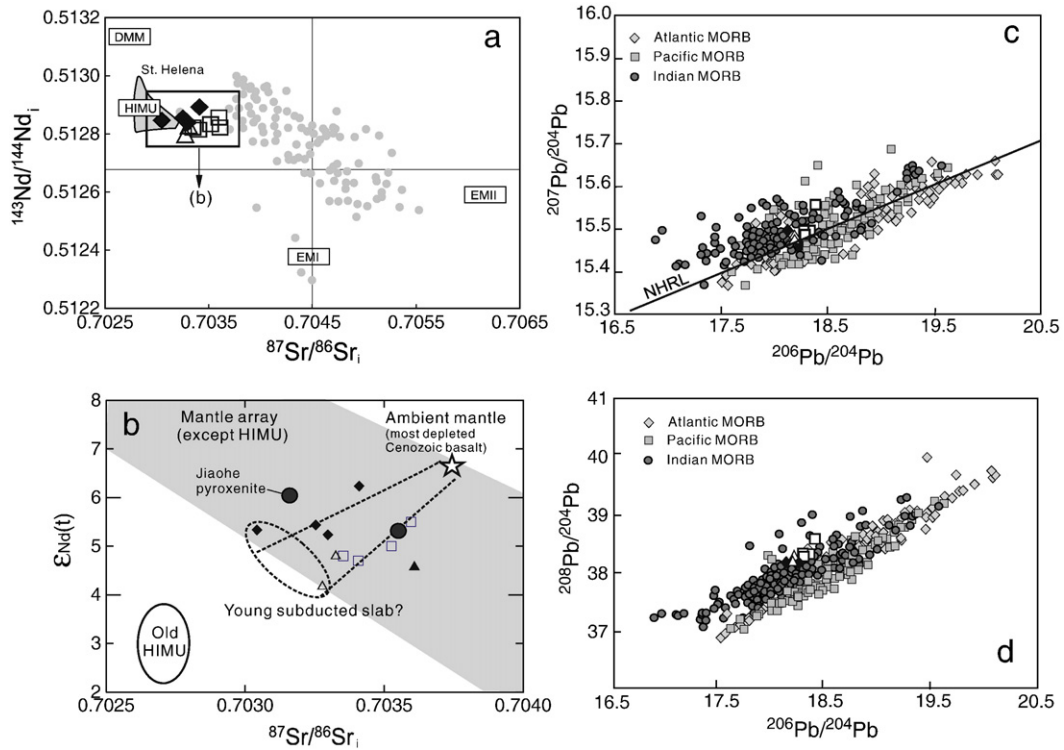**Fig. 7.** (a) $(^{87}Sr/^{86}Sr)_i$ versus $(^{143}Nd/^{144}Nd)_i$; (b) enlarged box area in a; (c) $^{207}Pb/^{204}Pb$ versus $^{206}Pb/^{204}Pb$, and (d) $^{208}Pb/^{204}Pb$ versus $^{206}Pb/^{204}Pb$ for the Shuangliao basalts. Data for Chinese Cenozoic basalts are shown in a by gray dots for comparison. Garnet pyroxenites from Jiaohe, which are interpreted as young recycled oceanic crust (Yu et al., 2010), are shown in b. Data sources as in Fig. 6. The fields of MORB, EM1, EM2, HIMU and the Northern Hemisphere Reference Line (NHRL) are taken from Hart (1984), Zindler and Hart (1986) and Hanyu et al. (2011). Data for Pacific, Indian and Atlantic MORB in (c–d) are from Hofmann (2004). Note the resemblance of the Shuangliao basalt to Indian MORB rather than to Pacific MORB.

(a) In a metasomatized upper mantle, alkalis (e.g. K, Rb, Ba) and water are commonly stored in amphibole and phlogopite and are retained in these minerals relative to anhydrous minerals during melting. This implies a lithospheric source (i.e., Halliday et al., 1990; Class and Goldstein, 1997), because amphibole and phlogopite are only stable in the lithospheric mantle rather than in convective
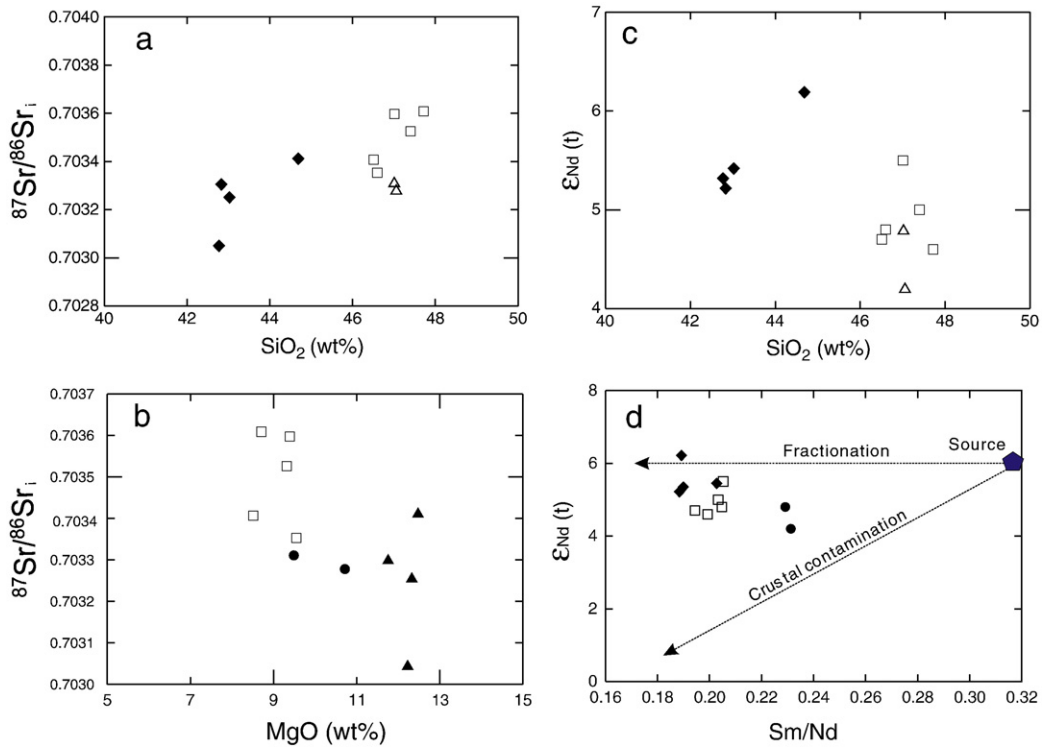
Fig. 8. (a) $(^{87}Sr/^{86}Sr)_i$ versus SiO_2; (b) $(^{87}Sr/^{86}Sr)_i$ versus MgO; (c) $\varepsilon_{Nd}(t)$ versus SiO_2; and (d) $\varepsilon_{Nd}(t)$ versus Sm/Nd. Symbols as in Fig. 4.
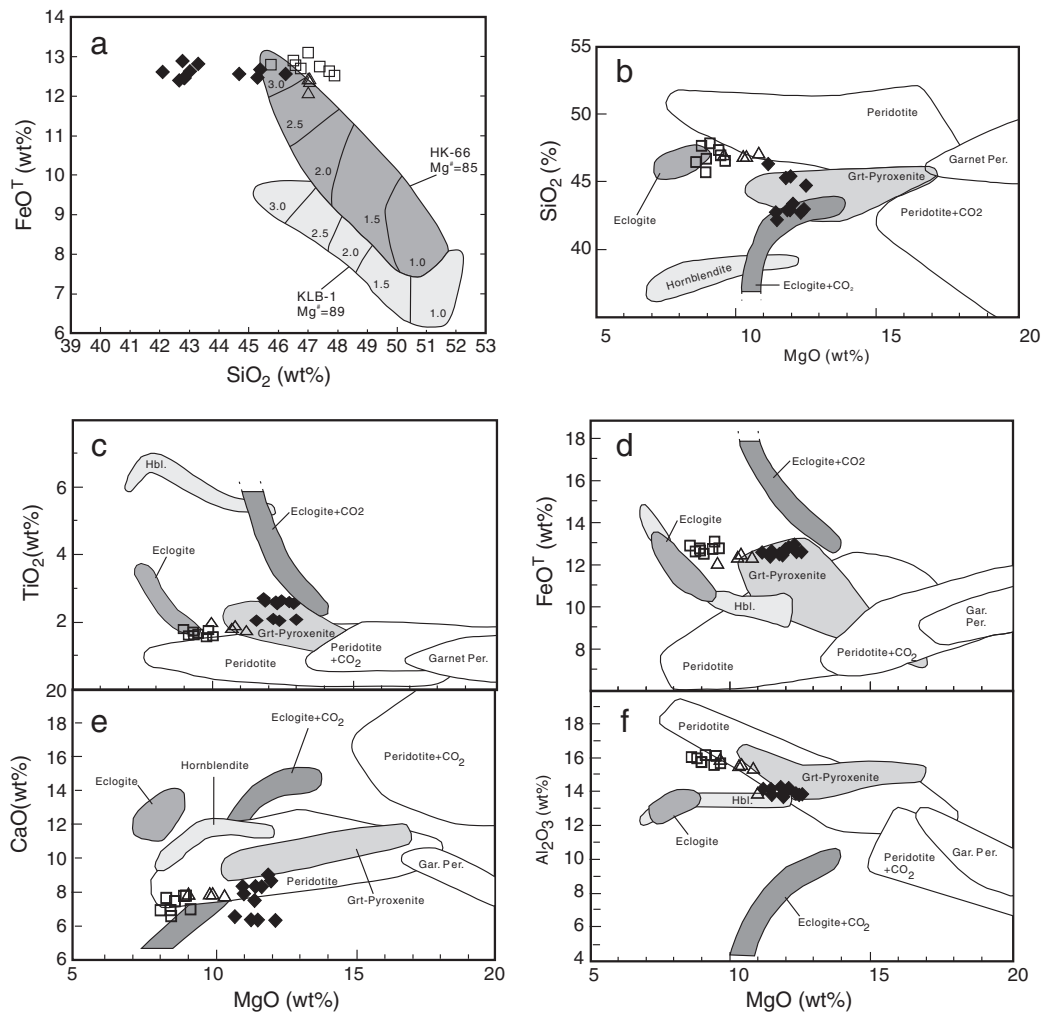
Fig. 9. Comparison of the Shuangliao basalts with high-pressure experimental melts of various starting materials. (a) SiO_2 versus FeOt; (b–f) SiO_2, TiO_2, FeO, CaO and Al_2O_3 versus MgO. Data source: volatile-free peridotite (Hirose and Kushiro, 1993; KLB-1 is refractory peridotite with mg-number 89, whereas HK-66 is fertile with mg-number 85), peridotite + CO_2 (Dasgupta et al., 2007), dry (Kogiso and Hirschmann, 2006) and carbonated eclogite (Dasgupta et al., 2006), of garnet pyroxenite (Hirschmann et al., 2003) and of hornblendite (Pilet et al., 2008). Numbers in small letters in a denote pressure in GPa.

asthenosphere. If metasomatized lithosphere is a direct source of al-kaline magmas, residues of amphibole and phlogopite after small de-grees of partial melting may account for the negative K-anomalies on multi-element spider diagram (Class and Goldstein, 1997) and deple-tion of U, Th, Rb, Ba relative to Nb. However, given the high partition coefficients of Nb and Ti (Ionov and Hofmann, 1995), amphibole and phlogopite residues in magma source can equally generate depletion of Nb and Ta in the melts, a feature not observed in the Shuangliao samples.

Similar problems are encountered by hornblendite as the source of alkaline volcanic rocks (Pilet et al., 2008). Pilet et al. (2005) argued that peridotites, veined by intermediate-mafic materials can generate HIMU-type basalts, which inherit the composition of Nb-rich mineral-bearing intermediate veins that are characterized by low LILE and high Nb–Ta contents. However, Nb-rich minerals could also host Zr and Hf, thereby producing positive Zr and Hf anomalies. No such anomalies are observed for the Shuangliao basalts. In addition, the ex-perimental melts of hornblendite are too low in MgO, FeOt and Na_2O to be the parental melt of the Shuangliao basalts (see Fig. 9).

Information as to the composition of the lithospheric mantle be-neath Shuangliao is available from studies of the peridotite xenoliths carried by the alkali basalts (Wu et al., 2003; Yu et al., 2009). If the Shuangliao basalts originated from the lithospheric mantle, they like-ly inherited the characteristics of peridotites. The peridotite xenoliths

from Shuangliao are essentially anhydrous, and lack metasomatic phases such as amphibole and phlogopites (Wu et al., 2003; Yu et al., 2009). Most of the peridotites show enrichment of incompatible elements with relatively depletion in Nb and Ta compared to the neighboring elements on the spider diagram. As shown by Yu et al. (2009) for the Shuangliao peridotites, and by others (e.g., Bedini et al., 1997; Xu et al., 1998) for peridotites from many other localities, LILE-enriched peridotites generally show lower ε_{Nd} and higher $^{87}Sr/^{86}Sr$ than the LILE-depleted samples. Specifically in the Shuangliao case, $^{87}Sr/^{86}Sr$ of metasomatized peridotites ranges from 0.7030 to 0.7070, ε_{Nd} from −1.3 to 8.7, whereas "unmetasomatized" samples have $\varepsilon_{Nd} > 11$ and $^{87}Sr/^{86}Sr < 0.7030$. This reflects either mixing with an enriched melt component or time-integrated radiogenic evolution after the enrichment processes. If the Shuangliao basalts were derived from a metasomatized source, they are expected to have relatively low ε_{Nd} and high $^{87}Sr/^{86}Sr$. However $(^{87}Sr/^{86}Sr)_i$ of the Shuangliao basalts vary between 0.7030 and 0.7036, significantly lower than those for the LILE-enriched peridotites from the same localities.

The final concern with a metasomatized lithospheric source is their low La/Nb ratios, which are very high in arc-related volcanics and volcanic rocks of hydrated lithosphere (e.g., Cordilleran).

(2) In the model of recycled metasomatized lithosphere (Niu and O'Hara, 2003), amphibole and phlogopite are no longer stable and will breakdown at high pressure (>3 GPa). The absence of these
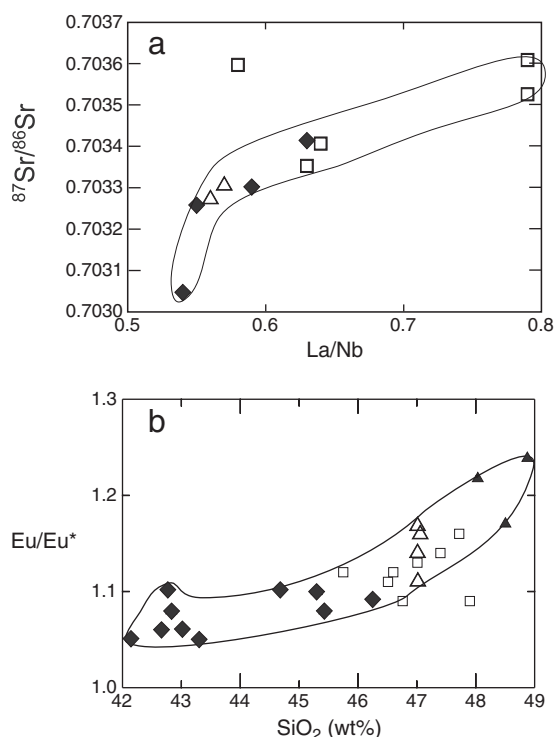
Fig. 10. (a) $(^{87}Sr/^{86}Sr)_i$ versus La/Nb; (b) Eu/Eu* versus SiO_2.

phases in the source solves the problem (Nb–Ta enrichment versus depletion) encountered by the model involving the metasomatized lithosphere as a direct magma source, but it presents a problem for the depletion of very highly incompatible elements such as K, Rb, Ba, Th, U. This implies a different source other than lithospheric mantle for the Shuangliao Eocene lavas.

5.3.3. Young recycled oceanic crust?

The elimination of the metasomic model leaves us with a recycled oceanic crust model, which is supported by several lines of evidence as follows.

(a) The depletion of the highly incompatible elements (Rb to U) relative to the REE and the enrichment of most other trace elements with respect to the Bulk Silicate Earth in the source of the Shuangliao basalts suggests that they are most likely produced by melting of very incompatible elements and LREE-depleted precursors. Oceanic crust represents the most suitable candidate for this source, because subducted oceanic lithosphere (basaltic crust plus oceanic lithospheric mantle) is the only known component that is depleted in very incompatible elements (Hofmann, 2004; Stracke et al., 2005).

Sr and Nd isotopes of the Shuangliao basanites and other lavas define two subparallel trends with positive slopes (Fig. 7b), in contrast with the negative correlation exhibit by the majority of Cenozoic basalts from eastern China (Fig. 7b). The positive Sr–Nd correlation might reflect mixing between a HIMU end-member (low $^{87}Sr/^{86}Sr$ and low ε_{Nd}) and the sub-continental mantle, which is represented by the most depleted Cenozoic basalts (Fig. 7a,b). This is consistent with low La/Nb coupled with low $^{87}Sr/^{86}Sr$ in recycled oceanic crust (Fig. 10a). The previously published Sr–Nd isotopic range for St. Helena basalts overlaps with the data points of Shuangliao lavas (Fig. 7a). However, Hanyu et al. (2011) recently showed that slightly high $^{87}Sr/^{86}Sr$ in some HIMU lavas may be due to alteration and that HIMU lavas exhibit very uniform and unradiogenic $^{87}Sr/^{86}Sr$ (~0.7028, Fig. 7b). Therefore, "old" HIMU may not be a suitable source for the Shuangliao lavas. A young subducted oceanic slab is thus

inferred (Fig. 7b). It gains support from comparison of the Shuangliao basalts with the garnet pyroxenite xenoliths from Jiaohe, NE China, which have recently been interpreted as remnants of young subducted oceanic crust (Yu et al., 2010). The Jiaohe pyroxenites show a wider Sr–Nd isotopic range than the Shuangliao basalts, but the samples with the lowest $^{87}Sr/^{86}Sr$ overlap with the Shuangliao basalts in Fig. 7b. This, in conjugation with their unradiogenic Pb isotopic ratios, supports the presence of young SOC in the source of the Shuangliao basalts.

(b) The positive Eu and Sr anomalies are present not only in moderately fractionated transitional basalts, but also in magnesian basanites which seem to have been subjected to little fractionation. These anomalies thus most likely reflect source characteristics, in which plagioclase was a significant component. The oceanic crust, constituted by MORB-type basalts and underlying gabbroic/ultramafic cumulates, is therefore a plausible candidate for this plagioclase-rich source. It is noted from Fig. 5 that positive Eu anomaly becomes more significant with decreasing alkalinity, from basanite, through alkaline olivine basalts to transitional basalts. This is further illustrated by a rough positive correlation between Eu/Eu* and SiO_2 (Fig. 10b), implying a source of upper and lower oceanic crust for basanites and AOB, and a dominantly lower oceanic crust for transitional basalts and diabases. The idea that different layers of subducted oceanic lithosphere could be responsible for the geochemical variations in magmas receives support from recent studies of Hawaiian, Icelandic and Maeira hotspot volcanism (Hauri, 1996; Chauvel and Hemond, 2000; Geldmacher and Hoernle, 2000).

(c) As a result of subduction and deep mantle recycling, oceanic crustal material will be transformed into garnet pyroxenite/eclogite. A source lithology with this composition is consistent with the inferences drawn from the comparison of the Shuangliao basalt data with experimental data (Fig. 9) and the findings from the garnet pyroxenite xenoliths, which are interpreted as remnants of oceanic lower crust (Yu et al., 2010). Less well constrained is whether different layers of subducted oceanic lithosphere are transformed to different lithology (garnet pyroxenites versus eclogite). In the following discussion, the term garnet pyroxenites/eclogite is used to designate components derived from SOC.

5.4. Origin of the Shuangliao basalts — melting of an upwelling heterogeneous asthenosphere

The previous discussion suggests that the source of the Shuangliao basalts is heterogeneous, consisting of fusible pyroxenites/eclogites and refractory peridotites. Melting of this upwelling heterogeneous asthenosphere, especially if lithospheric thinning (Menzies et al., 1993; Xu, 2001) is taken into account, can explain the decreasing alkalinity of the Shuangliao lavas with time. During upwelling of this type of mantle, the solidus for the hydrothermally altered, oceanic crust and its metamorphosed products (upper oceanic crust) was crossed first, followed by the solidus for gabbroic lower oceanic crust and then by peridotitic mantle (Fig. 11). It is possible that at ~50 Ma, the lithosphere was relatively thick so that the melting column was largely confined to the deep mantle. Under these circumstances, only the recycled crustal components (i.e., eclogite/pyroxenite) with low melting points start to melt, generating basanites and alkali basalts (Fig. 11a). The result is pooled melts that are derived from both the upper and lower oceanic crust. Due to the lower melting temperature of the upper oceanic crust, compared to cumulate lower oceanic crust, the basanites would trap more upper oceanic crust, accounting for their relatively low Eu/Eu*. With progressive lithospheric thinning, the melting column moved to a relatively shallow level. As a consequence, relatively large degree melting took place to, generate the transitional basalts (Fig. 11b). Due to consumption of a significant volume of upper oceanic crust in earlier melting events, melts generated during this period are dominantly from the lower oceanic crust,
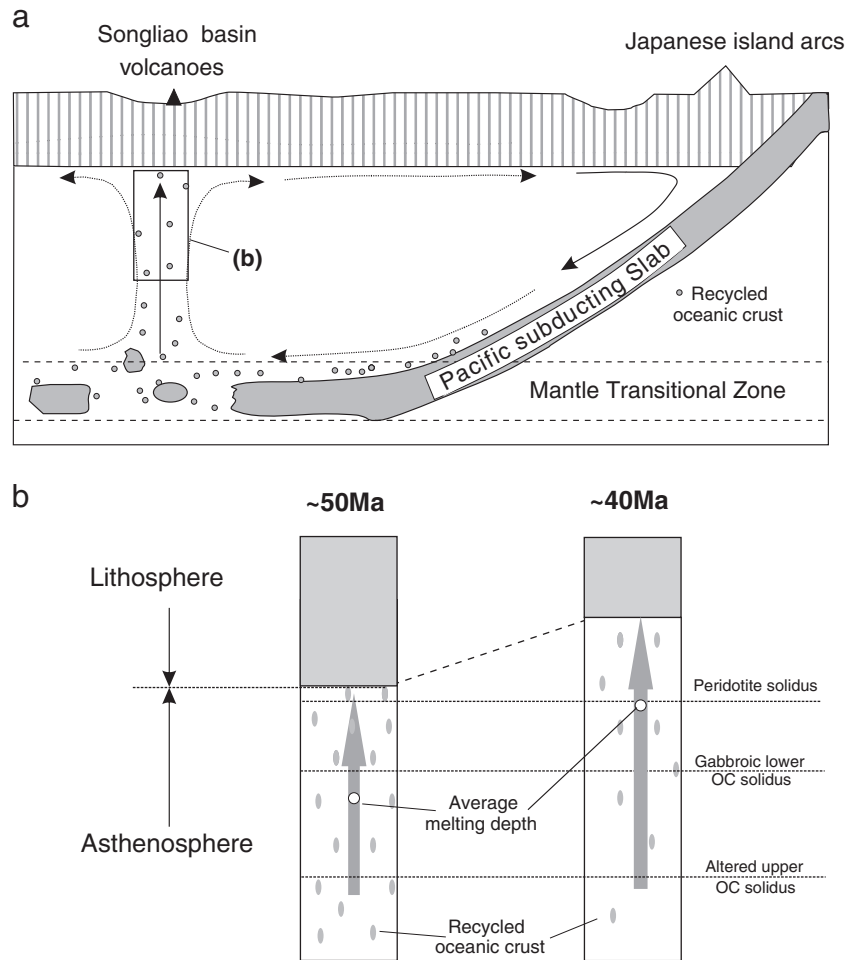
Fig. 11. Cartoon illustrating subducted oceanic crust (SOC) components in the Shuangliao basalts, and melting of upwelling heterogeneous asthenosphere during lithosphere thinning. (a) Subduction of Pacific plate underneath the Asian continent (Huang and Zhao, 2006) induced upper mantle convection and back-arc extension. Upwelling mantle flows were focused along lithospheric weak zones (i.e., Tanlu fault and edge of the Songliao basin). The upwelling mantle flux consists of SOC components, probably derived from the stagnant oceanic slabs in the mantle transition zone. (b) Change in melting columns explains the temporal decrease in alkalinity and proportion of different layers of SOC in the Shuangliao basalts. At ~50 Ma, the lithosphere was relatively thick and the melting column was largely confined to the deep mantle, where only low melting point SOC components (i.e., eclogite/pyroxenite) can melt to generate highly alkaline basalts. The resultant melts are mixture of melts from both upper and lower oceanic crust, accounting for their relatively low Eu/Eu*. At ~40 Ma, the melting column moved to a relatively shallow level, both peridotites and SOC melt to generate transitional basalts and sub-alkaline diabases. Due to consumption of upper oceanic crust in previous melting events, the resultant melts during this period are dominated by those from the gabbroic lower crust, accounting for their high Eu/Eu*.

accounting for their relatively high Eu/Eu*. The ambient mantle may also have participated in these melting events, but in a subordinate way.

5.5. Oceanic crustal components from the mantle transition zone?

In this section we discuss the provenance of the recycled oceanic crust. It has widely been accepted that oceanic crust can be recycled through the mantle as a result of subduction to a thermal boundary layer and then subsequent return to the surface at mid ocean ridges or hotspots. However, there is no evidence from recent seismic studies for mantle plumes underneath eastern China (Huang and Zhao, 2006; Chen, 2010).

Two potential models are considered here. The first involves dispersed oceanic crust in the convective mantle (like the plum-pudding model), which is widely proposed for the source of small-scale alkali volcanism. In this scheme, recycling of components may operate in a large scale and their provenance is almost impossible to constrain. Nevertheless, such crust may be old, and therefore inconsistent with the unradiogenic Pb isotopes and higher $^{87}Sr/^{86}Sr$ relative to type HIMU lavas in case of Shuangliao lavas.

Alternatively, the young SOC required for the Shuangliao basalt source may have been derived from stagnant Pacific oceanic slabs identified in the mantle transition zone (MTZ) beneath the East Asian continent (Fukao et al., 1992; Zhao et al., 2004; Huang and Zhao, 2006). Plate reconstruction by Mueller et al. (2008) suggests that subduction of the Pacific plate underneath the Asian continent was initiated by the Early Cretaceous. Niu (2005) and Van der Hilst and Li (2011) estimated that the subducting slab may have existed beneath eastern China during the late Cretaceous. In this scenario, the mantle underneath eastern China is stratified at the time of Shuangliao magmatism, with a horizontal slab in the mantle transition zone separating the upper and lower mantle. As a consequence, whole mantle convection does not reach the very shallow levels beneath China and, as a consequence, cannot produce plume-related volcanism. An implication is that the recycled crust components in the Shuangliao basalts cannot be derived from the core–mantle boundary.

It has been shown that at pressure comparable to that of the mantle transition zone, subducted oceanic crusts will consist of stishovite, majorite and hollandite (Irifune et al., 1994), and that hollandite $(KAlSi_3O_8)$ can readily host the large ion lithophile elements. K variation in the Shuangliao basalts can be best understood if their

source contains small amount of hollandite in the mantle transition zone. It is noted from Fig. 5 that negative K anomaly is present in Shuangliao basanites, but not in the AOB and transitional basalts. The basanites appear to be the lowest degree partial melts based on their higher abundances of most trace elements; the low K contents can be due to presence of a hollandite structure mineral at very low melt fractions. However such a phase may melt out at the higher partial melt fractions that created AOB and transitional basalts.

If the SOC in the Shuangliao lavas were derived from the stagnant slab related to subduction of Pacific slab, it should isotopically resemble the Pacific MORB. However, the relatively low $^{87}Sr/^{86}Sr$ and $^{143}Nd/^{144}Nd$ of the Shuangliao basalts does not match that of Pacific MORB. Although this may be accounted for by addition of small amount of sediment to oceanic crust, the fact that Shuangliao lavas are distinct from Pacific MORB but similar to Indian MORB in terms of Pb isotopes (Fig. 7c–d) presents a challenge to this alternative. This dilemma can be reconciled if the slab that currently stagnated beneath eastern China has a more Indian MORB affinity than Pacific MORB. Although no Indian-type ocean crust has been found in the northwestern Pacific, Straub et al. (2009) noticed the discrepancy in the present-day Izu-Bonin trench input (Pacific oceanic crust) and arc output (Indian crust signature). On the basis of plate tectonic reconstructions and Pb isotopes of arc magmas at Kuriles, they suggested that old (~120 Ma) subducted slab of Izanaghi–Pacific plate in NW Pacific would have Indian-type crust composition. This type plate is mostly extinct from the surface at present, with possible remnant at Kuriles arc (Straub et al. 2009). We thus speculate that the stagnated beneath the eastern Asian continent is of Indian MORB type rather than of Pacific MORB. The melting of recycled oceanic crust derived from such a stagnant slab therefore accounts the Indian-type mantle signature of the Shuangliao intraplate basalts, and perhaps the widespread Dupal anomaly observed in Cenozoic basalts in eastern China (Tu et al., 1991).

6. Conclusions

1. Ar–Ar radiometric dating shows that volcanic eruption at the Shuangliao, NE China, took place at 41–51 Ma. There are an apparent decrease in the alkaline content with time, from strong alkaline basanites at ~50 Ma to olivine basalts to transitional basalts at 41–43 Ma and finally subalkaline diabases.
2. The Shuangliao Eocene basalts are characterized by high FeO contents, low Sr isotopic ratios, negative K anomalies, positive Nb–Ta anomalies, and weak positive Eu and Sr anomalies. The general enrichment of incompatible trace elements and the depletion of very incompatible trace elements are typical HIMU characteristics. This is attributed to presence of young SOC in the source of Shuangliao basalts. If this interpretation is correct, the high FeO content, and positive Eu and Sr anomalies can also be used as criteria to identify recycled oceanic crust in the source of a given basalt.
3. The SOC components in the Shuangliao basalts are likely derived from the stagnant Pacific slab within the mantle transition zone beneath eastern China. The Indian MORB-like isotopic composition of this SOC is consistent with Indian-type crust composition of the extinct Izanaghi–Pacific plate. Therefore this study provides evidence for the involvement of subduction of Pacific plate in genesis of Cenozoic intraplate magmatism in eastern China, and by inference, its role in the lithospheric thinning processes.
4. The geochemistry of the Shuangliao basalts can be best understood by melting of a heterogeneous asthenosphere consisting of recycled oceanic crust and mantle peridotites, especially in conjugation with lithospheric thinning processes.

References

Basu, A.R., Wang, J.W., Huang, W.K., Xie, G.H., Tatsumoto, M., 1991. Major element, REE and Pb, Nd and Sr isotopic geochemistry of Cenozoic volcanic rocks of eastern China: implications for origin from suboceanic-type mantle reservoirs. Earth and Planetary Science Letters 105, 149–169.

Bedini, R.M., Bodinier, J.-L, Dautria, J.M., Morten, L., 1997. Evolution of LILE-enriched small melt fractions in the lithospheric mantle: a case study from the Eastern African Rift. Earth and Planetary Science Letters 153, 67–83.

Chaffey, D.J., Cliff, R.A., Wilson, B.M., 1989. Characterization of the St. Helena magma source. In: Saunders, A.D., Norry, M.J. (Eds.), Magmatism in the Ocean Basins, 42. Geological Society Special Publication, London, pp. 257–276.

Chauvel, C., Hemond, C., 2000. Melting of a complete section of recycled oceanic crust: trace element and Pb isotopic evidence from Iceland. Geochemistry, Geophysics, Geosystems 1 (1999GC000002).

Chauvel, C., Hofmann, A.W., Vidal, P., 1992. HIMU-EM: the French Polynesian connection. Earth and Planetary Science Letters 110, 99–119.

Chen, L., 2010. Concordant structural variations from the surface to the base of the upper mantle in the North China Craton and its tectonic implications. Lithos 120, 96–115.

Chen, J.C., Hsu, C.N., Ho, K.S., 2003. Geochemistry of Cenozoic volcanic rocks and related ultramafic xenoliths from the Jilin and Heilongjiang provinces, northeast China. Journal of Asian Earth Sciences 21, 1069–1084.

Chen, Y., Zhang, Y.X., Graham, D., Su, S.G., Deng, J.F., 2007. Geochemistry of Cenozoic basalts and mantle xenoliths in Northeast China. Lithos 96, 108–126.

Class, C., Goldstein, S.L., 1997. Plume–lithosphere interactions in the ocean basins: constraints from the source mineralogy. Earth and Planetary Science Letters 150, 245–260.

Dasgupta, R., Hirschmann, M.M., Stalker, K., 2006. Immiscible transition from carbonate rich to silicate-rich melts in the 3 GPa melting interval of eclogite + CO_3 and genesis of silica-undersaturated ocean island lavas. Journal of Petrology 47, 647–671.

Dasgupta, R., Hirschmann, M.M., Smith, N.D., 2007. Partial melting experiments of peridotite + CO_2 at 3 GPa and genesis of alkalic ocean island basalts. Journal of Petrology 48, 2093–2124.

Dasgupta, R., Jackson, M.G., Lee, C.T., 2010. Major element chemistry of ocean island basalts — conditions of mantle melting and heterogeneity of mantle source. Earth and Planetary Science Letters 289, 377–392.

Fan, Q., Hooper, P., 1991. The Cenozoic basaltic rocks of eastern China: petrology and chemical composition. Journal of Petrology 32, 765–810.

Frey, F.A., Green, D.H., Roy, S.D., 1978. Integrated models of basalt petrogenesis: a study of quartz tholeiites to olivine melilitites from southeastern Australia utilizing geochemical and experimental petrological data. Journal of Petrology 19, 463–513.

Fukao, Y., Obayashi, M., Inoue, H., Nenbai, M., 1992. Subducting slab stagnant in the mantle transition zone. Journal of Geophysical Research 97, 4809–4822.

Geldmacher, J., Hoernle, K., 2000. The 72 Ma geochemical evolution of the Madera Hotspot (eastern North Atlantic); recycling of Paleozoic (<500 Ma) oceanic lithosphere. Earth and Planetary Science Letters 183, 73–92.

Goto, A., Tatsumi, Y., 1996. Quantitative analyses of rock samples by an X-ray fluorescence spectrometer (II). The Rigaku Journal 13, 20–39.

Green, D.H., Ringwood, A.E., 1967. The "genesis" of basaltic magmas. Contributions to Mineralogy and Petrology 15, 103–109.

Halliday, A.N., Davison, J.P., Holden, P., Dewold, C., Lee, D.C., Fitton, J.G., 1990. Trace-element fractionation in plumes and the origin of HIMU mantle beneath the Cameroon Line. Nature 347, 523–528.

Hanyu, T., Tatsumi, Y., Senda, R., Miyazaki, T., Chang, Q., Hirahara, Y., Takahashi, T., Kawabata, H., Suzuki, K., Kimura, J.-I., 2011. Geochemical characteristics and origin of the HIMU reservoir: a possible mantle plume source in the lower mantle. Geochemistry, Geophysics, Geosystems 12 (2). doi:10.1029/2010GC003252.

Hart, S.R., 1984. A large-scale isotope anomaly in the Southern Hemisphere mantle. Nature 309, 753–757.

Hauri, E.H., 1996. Major element variability in the Hawaiian mantle plume. Nature 382, 415–419.

Hirose, K., Kushiro, I., 1993. Partial melting of dry peridotites at high pressures: determination of compositions of melts segregated from peridotite using aggregates of diamond. Earth and Planetary Science Letters 114, 477–489.

Hirschmann, M.M., Stopler, E.M., 1996. A possible role for garnet pyroxenite in the origin of the garnet signature in MORB. Contributions to Mineralogy and Petrology 124, 185–208.

Hirschmann, M.M., Kogiso, T., Baker, M.B., Stolper, E.M., 2003. Alkalic magmas generated by partial melting of garnet pyroxenite. Geology 31, 481–484.

Hofmann, A.W., 2004. Sampling mantle heterogeneity through oceanic basalts: isotopes and trace elements. In: Carlson, R.W. (Ed.), Treatise on Geochemistry. The mantle and core, Vol. 2. Elsevier, New York, pp. 61–101.

Hofmann, A.W., White, W.M., 1982. Mantle plumes from ancient oceanic crust. Earth and Planetary Science Letters 57, 421–436.

Huang, J.L., Zhao, D.P., 2006. High-resolution mantle tomography of China and surrounding regions. Journal of Geophysical Research 111, B09305.

Ionov, D.A., Hofmann, A.W., 1995. Nb–Ta-rich mantle amphiboles and micas: implications for subduction-related metasomatic trace element fractionations. Earth and Planetary Science Letters 131, 341–356.

Irifune, T., Ringwood, A.E., Hibberson, W.O., 1994. Subduction of continental-crust and terrigenous and pelagic sediments — an experimental-study. Earth and Planetary Science Letters 126, 351–368.

Jolivet, L., Tamaki, K., Fournier, M., 1994. Japan Sea, opening history and mechanism: a synthesis. Journal of Geophysical Research 99, 22,237–22,259.

Kogiso, T., Hirschmann, M.M., 2006. Partial melting experiments of bimineralic eclogite and the role of recycled mafic oceanic crust in the genesis of ocean island basalts. Earth and Planetary Science Letters 249, 188–199.

Kogiso, T., Tatsumi, Y., Shimoda, G., Barsczus, H.G., 1997. High μ (HIMU) ocean island basalts in southern Polynesia: new evidence for whole mantle scale recycling of subducted oceanic crust. Journal of Geophysical Research 102 (B4), 8085–8103.

Kogiso, T., Hirschmann, M.M., Frost, D.J., 2003. High-pressure partial melting of garnet pyroxenite: possible mafic lithologies in the source of ocean island basalts. Earth and Planetary Science Letters 216, 603–617.

Koppers, A.A.P., 2002. ArArCALC — software for ^{40}Ar/^{39}Ar age calculations. Computers and Geosciences 28, 605–619.

Kushiro, I., 2001. Partial melting experiments on peridotite and origin of mid-ocean ridge basalt. Annual Review of Earth and Planetary Sciences 29, 71–107.

Langmuir, C.H., Klein, E.M., Plank, T., 1992. Petrological systematics of mid-ocean ridge basalts: constraints on melt generation beneath ocean ridges. In: Morgan, J.P., Blackman, D.K., Sinton, J.M. (Eds.), Mantle Flow and Melt Generation at Mid-ocean Ridges, 71. Geophys Monogr Series, Washington DC, pp. 81–180.

Le Bas, M.J., Le Maitre, R.W., Strekeisen, A., et al., 1986. chemical classification of volcanic rocks based on the total alkali–silica diagram. Journal of Petrology 27, 745–750.

Liang, X.R., Wei, G.J., Li, X.H., Liu, Y., 2003. Precise determination of ^{143}Nd/^{144}Nd and Sm/Nd isotopes using MC-ICPMS. Geochimica 32, 91–96.

Liu, R.X., Chen, W.J., Sun, J.Z., Li, D.M., 1992. The K–Ar age and tectonic environment of Cenozoic volcanic rock in China. In: Liu, R.X. (Ed.), The Age and Geochemistry of Cenozoic Volcanic Rock in China. Seismologic Press, Beijing, pp. 1–43.

Liu, J.Q., Han, J.T., Fyfe, W.S., 2001. Cenozoic episodic volcanism and continental rifting in northeast China and possible link to Japan Sea development as revealed from K–Ar geochronology. Tectonophysics 339, 385–401.

McDonald, G.A., Katsura, T., 1964. Chemical composition of Hawaiian Lavas. Journal of Petrology 5, 82–133.

Menzies, M.A., Fan, W.M., Zhang, M., 1993. Palaeozoic and Cenozoic lithoprobes and the loss of >120 km of Archaean lithosphere, Sino–Korean craton, China. In: Prichard, H.M., Alabaster, T., Harris, N.B.W., Neary, C.R. (Eds.), Magmatic Processes and Plate Tectonics, 76. Geol. Soc. Spe. Pub., London, pp. 71–78.

Mueller, R.D., Sdrolias, M., Gaina, C., Steinberger, B., Heine, C., 2008. Long-term sea-level fluctuations driven by ocean basin dynamics. Science 319, 1357–1362.

Niu, Y.L., 2005. Generation and evolution of basaltic magmas: some basic concepts and a new view on the origin of Mesozoic–Cenozoic basaltic volcanism in Eastern China. Geol. J. China Universities 11, 9–46.

Niu, Y., O'Hara, M.J., 2003. Origin of ocean island basalts: a new perspective from petrology, geochemistry, and mineral physics considerations. Journal of Geophysical Research 108 (B4), 2209. doi:10.1029/2002JB002048.

Pilet, S., Hernandez, J., Sylvester, P., Poujol, M., 2005. The metasomatic alternative for ocean island basalt chemical heterogeneity. Earth and Planetary Science Letters 236, 148–166.

Pilet, S., Baker, M.B., Stolper, E.M., 2008. Metasomatized lithosphere and the origin of alkaline lavas. Science 320, 916–919.

Putirka, K., Ryerson, F.J., Perfit, M., Ridley, W.I., 2011. Mineralogy and composition of oceanic mantle. Journal of Petrology 52, 279–3313.

Qiu, H.N., Jiang, Y.D., 2007. Sphalerite ^{40}Ar/^{39}Ar progressive crushing and stepwise heating techniques. Earth and Planetary Science Letters 256, 224–232.

Salters, V.J.M., Stracke, A., 2004. Composition of the depleted mantle. Geochemistry, Geophysics, Geosystems 5, Q05004.

Sengör, A., Natal'lin, B.A., Burtaman, V.S., 1993. Evolution of the Altaid tectonic collage and Palaeozoic crustal growth in Eurasia. Nature 364, 299–307.

Song, Y., Frey, F.A., Zhi, X., 1990. Isotopic characteristics of Hannuoba basalts, eastern China: implications for their petrogenesis and the composition of subcontinental mantle. Chemical Geology 88, 35–52.

Stracke, A., Bourdon, B., 2009. The importance of melt extraction for tracing mantle heterogeneity. Geochimica et Cosmochimica Acta 73, 218–238.

Stracke, A., Hofmann, A.W., Hart, S.R., 2005. FOZO, HIMU, and the rest of the mantle zoo. Geochemistry, Geophysics, Geosystems 6, Q05007. doi:10.1029/2004GC00824.

Straub, S., Goldstein, S.L., Class, C., Schmidt, A., 2009. Mid-ocean-ridge basalt of Indian type in the northwest Pacific Ocean basin. Nature Geoscience 2, 286–289.

Sun, S.S., McDonough, W.F., 1989. Chemical and isotopic systematics of oceanic basalts: implications for mantle composition and processes. In: Saunders, A.D., Norry, M.J. (Eds.), Magmatism in the Ocean Basins, 42. Geological Society Special Publication, London, pp. 313–345.

Tanaka, T., Togashi, S., Kamioka, H., et al., 2004. JNdi-1: a neodymium isotopic reference in consistency with LaJolla neodymium. Chemical Geology 168, 279–281.

Thirlwall, M.F., 1997. Pb isotopic and elemental evidence for OIB derivation from young HIMU mantle. Chemical Geology 139, 51–74.

Tu, K., Flower, M., Carlson, R.W., Zhang, M., Xie, G.H., 1991. Sr, Nd and PB isotopic compositions of Hainan basalts (south China): implications for a subcontinental lithosphere Dupal source. Geology 19, 567–569.

Van der Hilst, R.D., Li, C., 2011. Large scale tectonic framework of East Asia: interplay between India–Eurasia collision in west and subduction and trench roll-back in east. International Conference on Cratonic Formation and Destruction, Beijing.

Wei, G.J., Liang, X.R., Li, X.H., Liu, Y., 2002. Precise determination of Sr isotopes of solution and solid samples using (LP) MC-ICPMS. Geochimica 31, 295–299.

Willbold, M., Stracke, A., 2006. Trace element compositions of mantle end-members: implications for recycling of oceanic and upper and lower continental crust. Geochemistry, Geophysics, Geosystems 7 (4). doi:10.1029/2005GC001005.

Wu, F.Y., Walker, R.J., Ren, X., Sun, D., Zhou, X., 2003. Osmium isotopic constraints on the age of lithospheric mantle beneath northeastern China. Chemical Geology 196, 107–129.

Wu, F.Y., Lin, J.Q., Wilde, S.A., Zhang, X., Yang, J.H., 2005. Nature and significance of the Early Cretaceous giant igneous event in eastern China. Earth and Planetary Science Letters 233, 103–119.

Xu, Y.G., 2001. Thermo-tectonic destruction of the Archaean lithospheric keel beneath eastern China: evidence, timing and mechanism. Physics and Chemistry of the Earth (A) 26, 747–757.

Xu, Y.G., 2002. Evidence for crustal components in mantle source and constraints on recycling mechanism: pyroxenite xenoliths from Hannuoba, North China. Chemical Geology 182, 301–322.

Xu, Y.G., 2007. Diachronous lithospheric thinning of the North China Craton and formation of the Daxin'anling–Taihangshan gravity lineament. Lithos 96, 281–298.

Xu, Y.G., Ross, J.V., Mercier, J.-C.C., 1993. The upper mantle beneath the continental rift of Tanlu, eastern China: evidence for the intralithospheric shear zones. Tectonophysics 225, 337–360.

Xu, Y.G., Menzies, M.A., Vroon, P., Mercier, J.C.C., Lin, C.Y., 1998. Texture–temperature–Geochemistry relationship in the upper mantle as revealed from spinel peridotite xenoliths from Wangqing, NE China. Journal of Petrology 39, 469–493.

Xu, Y.G., Menzies, M.A., Thirlwall, M.F., Huang, X.L., Liu, Y., Chen, X.M., 2003. "Reactive" harzburgites from Huinan, NE China: products of lithosphere–asthenosphere interaction during lithospheric thinning? Geochimica et Cosmochimica Acta 67, 487–505.

Xu, Y.G., Ma, J.L., Frey, F.A., Feigenson, M.D., Liu, J.-F., 2005. Role of lithosphere–asthenosphere interaction in the genesis of Quaternary alkali and tholeiitic basalts from Datong, western North China Craton. Chemical Geology 224, 247–271.

Yu, Y., 1987. Cenozoic basalt from Qixingshan, Shuangliao, Jilin Province: its characteristic and origin study. Acta Petrologica Sinica 3, 55–62 (in Chinese with English abstract).

Yu, S.Y., Xu, Y.G., Huang, X.L., Ma, J.L., Ge, W.C., Zhang, H.H., Qin, X.F., 2009. Hf–Nd isotopic decoupling in continental mantle lithosphere beneath Northeast China: effects of pervasive mantle metasomatism. Journal of Asian Earth Sciences 35, 554–570.

Yu, S.Y., Xu, Y.G., Ma, J.L., Zheng, Y.F., Kuang, Y., Hong, L.B., Ge, W.C., Tong, L.X., 2010. Remnants of oceanic lower crust in the subcontinental lithospheric mantle: trace element and O isotope evidence from aluminous garnet pyroxenite xenoliths from Jiaohe, Northeast China. Earth and Planetary Science Letters 297, 413–422.

Zeng, G., Chen, L.-H., Hofmann, A.W., Xu, X.S., 2011. Crust recycling in the sources of two parallel volcanic chains in Shandong, North China. Earth and Planetary Science Letters 302, 359–368.

Zhang, M., Menzies, M.A., Suddaby, P., Thirlwall, M.F., 1991. EMI signature from within the post-Archaean subcontinental lithospheric mantle: isotopic evidence from the potassic volcanic rocks in NE China. Geochemical Journal 25, 387–398.

Zhang, M., Suddaby, P., O'Reilly, S.Y., Norman, M., Qiu, J.X., 2000. Nature of the lithospheric mantle beneath the eastern part of the Central Asian fold belt: mantle xenolith evidence. Tectonophysics 328, 131–156.

Zhang, H.H., Xu, Y.G., Ge, W.C., Ma, J.L., 2006. Geochemistry of late Mesozoic–Cenozoic basalts in Yitong–Datun area. Jilin Province and its implication. Acta Petrologica Sinica 22, 1579–1607.

Zhang, J.-J., Zheng, Y.-F., Zhao, Z.-F., 2009. Geochemical evidence for interaction between oceanic crust and lithospheric mantle in the origin of Cenozoic continental basalts in east-central China. Lithos 110, 305–326.

Zhao, X., Coe, R.T., Zhou, Y., Wu, H., Wang, J., 1990. New paleomagnetic results from northern China: collision and suturing with Siberia and Kazakhstan. Tectonophysics 181, 43–81.

Zhao, D., Lei, J., Tang, R., 2004. Origin of the Changbai intraplate volcano in Northeast China: evidence from seismic tomography. Chinese Science Bulletin 49, 1401–1408.

Zhi, X., Song, Y., Frey, F.A., Feng, J., Zhai, M., 1990. Geochemistry of Hannuoba basalts, eastern China: constraints on the origin of continental alkalic and tholeiitic basalt. Chemical Geology 88, 1–33.

Zhou, X.H., Armstrong, R.L., 1982. Cenozoic volcanic rocks of eastern China — secular and geographic trends in chemistry and strontium isotopic composition. Earth and Planetary Science Letters 59, 301–329.

Zindler, A., Hart, S.R., 1986. Chemical geodynamics. Annual Review of Earth and Planetary Sciences 14, 493–571.

Zou, H., Zindler, A., Xu, X., Qi, Q., 2000. Major, trace element, and Nd, Sr and Pb isotope studies of Cenozoic basalts in SE China: mantle sources, regional variations, and tectonic significance. Chemical Geology 171, 33–47.